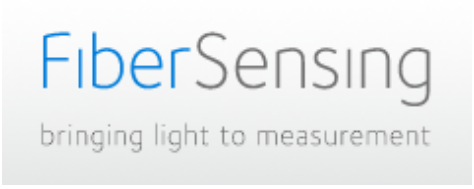

Optical fiber temperature sensors for cryogenic applications

Romão Azevedo Freitas

Mestrado Integrado em Engenharia Física

Departamento de Física e Astronomia

Orientador
Professor João Pedro Esteves de Araújo, Professor Associado ,
Faculdade de Ciências da Universidade do Porto

Coorientador
Doutor Francisco Moita Araújo , Director de Desenvolvimento de Produto,
FiberSensing- Sistemas Avançados de Monitorização

Acknowledgments

As the author of this report, I would like to use this opportunity to acknowledge the people who have helped me to develop this work.

My parents for financial and moral support that was ever present doing their best to help me succeed.

My girlfriend Rita for her never ending patience, understanding and moral support picking me up whenever I had a bad moment.

Professor Joao Pedro Araujo for his help, availability and interest facilitating everything I needed from IFIMUP-IN for experimental tests and measurements.

Doctor Francisco Araujo for providing me the opportunity to join FiberSensing and this very interesting project. For being available and allowing me to make my own decisions regarding to this project development and for providing all the materials and measuring devices needed for the optical measurements.

Doctor Ramalingam for allowing me to work with him in the Karlsruhe Institute for Technology, where the access to cryogenic liquids was easier and where a standard calibration facility was available for sensor testing and calibration.

Dr. José Monteiro for helping in all experimental testing done in FiberSensing and coaching me in the use of the BraggMeter being always available to help whenever I needed.

Dr. Luis Coelho for his help and availability, conducting all thing film depositions on the optical fibers. I would like to thank him also for sharing his knowledge regarding materials adhesion to the optical fibers and how to deposit them.

Dr. Arlete Apolinário for helping with everything related with the eletrodeposition of Ni and the Scanning Electron Microscopy analysis of the different coatings.

Dr. Goncalo Oliveira for helping with the tests done using the SQUID magnetometer teaching me how to operate the device. I would also like to thank him for his availability even at late hours.

I have been impressed with the urgency of doing. Knowing is not enough; we must apply. Being willing is not enough; we must do.

Leonardo da Vinci

Abstract

In this work studies are conducted to develop a cryogenic temperature sensor using Fiber Bragg Gratings (FBG).

Since bare FBG sensors only show sensitivity as temperature sensors above 80 K, coating techniques were used to increase the performance of these sensors at temperatures as low as 20K. The coating materials used in this project were metals like Mercury, Indium, Lead and Tin, all chosen due to their high Coefficient of Thermal Expansion in the temperature range between 20 and 80K.

In order to promote adhesion between the fiber and the coating, thin layers of Chromium and Titanium were deposited over the fiber. These metals were chosen due to their particular high adhesion to the fiber and high Young's Modulus (E).

Several deposition techniques were tested as coating methods, among them the Electron Beam Deposition proved to be the best technique to deposit the thin film buffers while casting proved to be the technique with the best results for the external coatings, due to the low melting points of the used metals.

All sensors created were tested and thermally trained between 4.2 and 80K and underwent calibration on a standard facility. Sensitivities of 14 pm/K were reached at 20K with some sensors. This sensitivity is high enough for the measuring equipment used (FS2200 BraggMETER) that has a resolution of 1pm, being thus our results very promising.

Table of Contents

Introduction

Temperature sensors are vital to a variety of everyday products. For example, household ovens, refrigerators, and thermostats rely on temperature maintenance and control in order to function properly. Temperature control also has applications in science and engineering, examples of this include the maintenance of the temperature of a reactor at the ideal set-point, monitoring the temperature of a possible runaway reaction to ensure personal safety, and maintaining the temperature of streams released to the environment to minimize harmful impact.

Humans generally sense temperature as “hot”, “warm”, or “cold”, however in science and engineering it is required precise, quantitative temperature measurements in order to accurately control a process. This is achieved through the use of temperature sensors, and temperature regulators which process the signals received from sensors.

From a thermodynamics perspective, temperature measures the average energy of chaotic molecular movements. As heat is added to a system, molecular motion increases and the system experiences an increase in temperature. It is difficult, however, to directly measure the energy of such molecular movement, so temperature sensors are generally designed to measure a property which changes in response to temperature. The devices are then calibrated to traditional temperature scales using a standard (like the boiling point of water at known pressure). [1]

The global market of temperature sensors is highly competitive, with a large number of players. Temperature is one of the most frequently measured parameters, with temperature sensors used in many industries (if not all). In fact, temperature applications are diverse, ranging from critical process control to maintaining comfort levels inside automobiles. There are several technologies that are used to measure temperature although temperature sensors can be broadly classified into two categories: contact and noncontact.

Contact temperature sensors, as the name suggests, must be in contact with the object whose temperature is being measured; it is assumed that the sensor and the object are in thermal equilibrium. Examples of contact temperature sensors include thermocouples, Resistance Temperature Detectors RTDs, thermistors, and Integrated Circuit (IC) sensors. Noncontact temperature sensors, such as infrared (IR) sensors, read a portion of the electromagnetic energy emitted by the object and then measure its intensity to determine temperature.

Some of the contact temperature sensor technologies have been present for decades and are considered mature and static. The noncontact temperature sensor technologies, in contrast, are more dynamic (still maturing) and are projected to show higher growth, given their increasing usage in a wide number of applications. Despite flat growth rates in certain technology segments, the overall temperature sensors and transmitters market is expected to grow during the 2011–2015 period, assuming the stable economic conditions in many emerging economies. Environmental legislation and demand from vertical market segments such as the automotive and telecommunications industries are expected to contribute as well to the growth of the temperature sensors and transmitters market.

Considering revenue generation for the global temperature sensor market for 2011, temperature sensor and transmitter used in the chemical and petrochemical industry represents the largest contribution with 19.3% to the total revenues in 2011 (Figure 1). Oil and gas, metallurgy, and automotive are the other key end-markets that generate sizable revenues for the worldwide market of temperature sensors and transmitters. These industries use most of the different types of temperature sensor technologies [2].

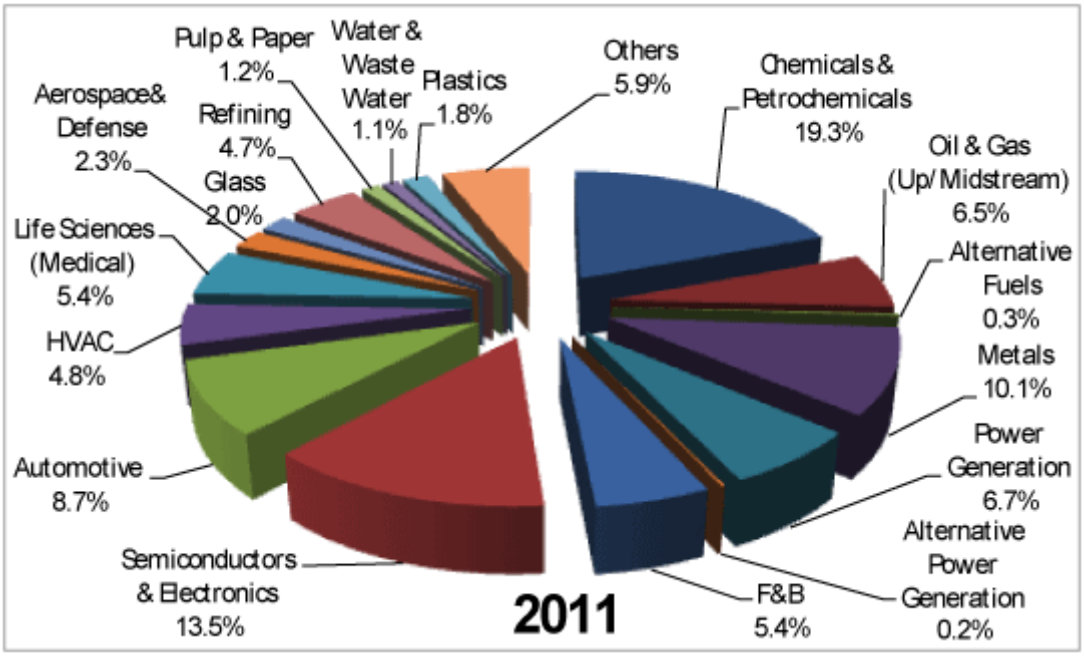

Figure 1 Revenue generation for the global temperature sensors market for 2011 [2]

Currently, there is a great use of temperature sensors especially with operating ranges close to room temperature due to the necessity of monitoring and control of electronic equipment. However, with the development of new technology is often necessary to

reach extremes in temperature. These limits are the source of major difficulties when building sensors, because physical properties of materials change radically relatively to those usual at room temperature. This is particularly true in the case of cryogenic applications in which decreasing temperature to near absolute zero alters the behavior of all materials. Their crystal structures become increasingly more compact and the lattice vibrations tend to cease, since the thermal energy is not enough to excite phonons. The temperature at which this change of behavior occurs is known as the "Debye Temperature" and is characteristic of each material. Thus, the lower this temperature is, the lower is the temperature below which the material´s physical properties become almost temperature independent.. It is thus difficult to find a good thermometric property below the Debye temperature of a given material.

In the most advanced research centers, such as those using large particle accelerators, in which cryogenic temperatures are essential for the proper functioning of unique equipment in the world of science and with extremely high financial value, sensors capable of operating in these temperature ranges are essential. They serve to monitor both the conditions of a complex set of equipment required to perform the experiments, and ensure the safety of the equipment itself.

Over the last two decades, optical fiber sensors have seen an increasing acceptance as well as widespread use for structural sensing and monitoring applications in civil engineering, aerospace, marine, oil & gas, composites and smart structures [3] [4]. Optical fiber sensor operation and instrumentation have become well understood and well developed.

Optical fiber sensors, especially FBGs, show distinguishing advantages like immunity to electromagnetic interference and power fluctuations along the optical path, high precision, durability, compact size, ease of multiplexing a large number of sensors along a single fiber, resistance to corrosion and reduced cable dimensions [5] [6] [7]. FBGs have become the most prominent sensors and are being increasingly accepted by engineers, as they are particularly attractive to perform strain and temperature measurements under harsh environment areas, like in the presence of electrical noise, EM interference and mechanical vibrations, where conventional sensors cannot operate. [8] Fiber-optic Bragg grating (FBG) sensors key research areas include FBG fabrication, FBG demodulation and practical applications [9] [10] [11].

Moreover, the fact that it is stimulated by light minimizes the power dissipation in the sample, while offering accuracy compatible with most applications. The response time

is potentially low given the small sensor-size. Moreover, nowadays the conditioning of the spectral signal can be easily processed with commercially available equipment.

These capabilities make this type of sensors a preferable solution for monitoring environments where high electromagnetic fields are needed, like that associated with infrastructures using superconducting magnets.

Motivation

Systems operating at cryogenic temperatures are becoming more and more important in the energy sector, transportation, and medical technology. Typical operation temperatures are given by the boiling points of Helium (4.2K) Hydrogen (20.3K) and Nitrogen (77.4K) although refrigerator cooling enables the operation at any temperature in the 3.7 K to 100K temperature range.

Materials applied in cryogenic systems, for example superconductors, are often very brittle, but conventional materials also change their properties when they are cooled down. On the other hand mechanical stress occurs during cooling or in superconducting magnets reacting to electro-magnetic forces. Therefore, beyond temperature control, monitoring the structural integrity is also an essential task in cryo-technology.

When working on an environment with cryogenic temperatures and high electro-magnetic fields there are limitations choosing the appropriate sensor type. When electrical sensors are used, the thermal conductivity of the signal wires (4 wires per measuring site) as well as magneto-resistance and parasitic voltages induced in strong magnetic fields (generation of strong magnetic fields can be assumed to be one of the main application of cryo-techniques) are common problems which are difficult to mitigate. For example it is already well known [12] that conventional resistance strain gauges (RSG) show increasing discontinuities in their strain-dependent electric resistance with decreasing temperature (between T = 20 K and 4.2 K). Also standard low temperature sensors, for example Si-diodes or resistors are influenced by magnetic fields. [13]

Low-temperature FBG sensors have potential application in temperature monitoring of superconducting magnet support structures where electric sparks are prohibited or electrical based sensors are susceptible to high magnetic field and radiation; in

spacecrafts which use liquid hydrogen-oxygen rocket engines whose parts are exposed to low temperatures, in the storage or transport vessels for cryogens or liquid hydrogen fuel tanks with high risk of ignition and also in particle physics experiments [14] [15]. However, it is well known that temperature sensitivity of bare FBG close to cryogenic temperatures is too low to be applied practically [16]. Enhancing the temperature sensitivity of FBGs is thus very significant not only for temperature sensing at cryogenic temperatures, but also to extend the use of this technology to broader sensing applications [17] [18].

The possible solution for the low sensitivity of these sensors due to silica's low Coefficient of Thermal Expansion (CTE) is to structurally attach the FBG to some material with a higher CTE, thus making the FBG sensor deformed by the hosting material. [19]

Objectives

This project has as main objective the development of a FBG sensor for cryogenic temperatures. This sensor should be capable to present a temperature sensitivity of at least 10pm/K in the range from 10 to 40 K.

To achieve this main goal, one envisages the increase of FBG sensitivity through coating with metals with high CTE, as well as to improve the adhesion between fiber and metal with thin metallic buffer layers.

Thus the determination of the best technique for sensor coating and the more cost effective needs to be carried out.

State of the art

Thermocouples are the temperature sensor of choice in many industries that require a stable sensor, featuring a fast response time, ease-of-use, low cost, and user familiarity. The chemical and petrochemical industries also use large numbers of RTDs because the sensors can operate in high-temperature and are compatible with challenging industrial environments. Infra-red (IR) sensors are used in several vertical

markets, including extensive use in the plastic, metals, and food and beverage industries and they are making inroads into process applications.

The process industries are becoming the largest purchases of IR temperature sensors where they are used for spotting defects and measuring surface temperature. The use of IR temperature sensors in the process industries is estimated to generate a 29.3% revenue share in 2011, with further growth expected by 2015 [2].

IR sensing in the food and beverage industry is used to detect immediate changes in temperature to lessen the risk of spoilage and reduce the chances of disease. Drivers for this market include government regulations, the need to minimize the amount of food wasted, and the need to reduce the number of batches rejected. The food and beverage industry's use of IR sensors is likely to contribute 5.4 % of the total temperature sensor revenue in 2011 [2].

IC temperature sensors are used in a variety of industries in applications that require small, low-cost sensors that provide accurate temperature measurement. The revenue from the temperature sensor usage in computers and consumer electronics dominates the total revenues of the IC temperature sensor market. Trends in the personal computing industry such as smaller system size, faster processors, and the need to support more powerful applications make monitoring and controlling heat imperative and this, coupled with robust sales of desktop and portable computers, is likely to continue to support this market. In 2011, IC temperature sensor applications in the semiconductors and electronics industries amounted to 13.5 % of the revenue of the total temperature sensors market [2].

Thermistors are used in automotive, HVAC (heating, ventilation, and air conditioning), medical, telecommunications, consumer electronics, and certain industrial applications. The process industries use fewer thermistors because of their narrow operating temperature range. The market for thermistors is expected to be driven by growth in the automotive market in the Asia Pacific region and in the emerging economies in Eastern Europe and Latin America, driven by an increased need for temperature measurement in vehicles for fuel efficiency and for passenger comfort. In the total temperature sensors market, thermistor use in automotive applications generates >8.7 % of the total revenue and thermistor use in HVAC applications generates 4.3% of the total revenue [2].

Noncontact temperature sensors, led by IR temperature sensors, are increasingly adopted for use in high-temperature applications. Several companies are investing in

research and development to improve the existing noncontact IR temperature sensing technologies and to develop newer ones. A number of companies, including tier-one automotive suppliers, have developed fixed IR temperature sensors to focus on markets that are currently dominated by thermocouples and RTDs. In the future, strong competition between contact and noncontact temperature sensing technologies is predictable. [2]

Conventional cryogenic sensors

Currently there are several sensors in the market capable of sensing very low temperatures of just a few Kelvin. Although they present a very interesting range for cryogenic usage they have several limitations regarding their usage under harsh environments. Table 1 represents the most common cryogenic temperature sensors in the market and their limitations.

Table 1– ***Cryogenic themperature sensors and theirs capabilities.*** [20]

	Temperature range	Standard curve	Below 1 K	Can be used in radiation	Performance in magnetic field
Diodes					
Silicon	1.4 K to 500 K	x			Fair above 60 K
GaAlAs	1.4 K to 500 K				Fair
Negative Temperature Coefficent RTDs					
Cernox™	0.10 K to 325 K		x	x	Excellent above 1 K
Germanium	0.05 K to 100 K		x	x	Not Recommended
Ruthenium Oxide (Rox™)	0.01 K to 40 K	x	x	x	Good below 1 K
Other					
Thermocouples	1.2 K to 1543 K	x			Fair
Capacitance	1.4 K to 290 K				Excellent
Positive Temperature Coefficient RTDs					
Platinum	14 K to 873 K	x		x	Fair above 30 K
Rhodium-Iron	0.65 K to 500 K		x	x	Fair above 77 K

Silicon

Silicon Diodes are the best choice for general-purpose cryogenic use. The cryogenic temperature sensors are interchangeable (they follow a standard curve) and are available in robust mounting packages and probes. Silicon Diodes are easy and inexpensive to instrument, and are used in a wide variety of cryogenic applications, such as cryo-coolers, laboratory cryogenics, cryo-gas production, and space satellites. [20]

GaAlAs

GaAlAs Diodes offer high sensitivity over a wide range of use (1.4 K to 500 K). They are useful in moderate magnetic fields, and offer many of the advantages of Silicon Diodes—easy to instrument, wide range, and robust packaging. They do not follow a standard curve. GaAlAs diodes are used in applications when instrumentation constraints (e.g., legacy installations, cost) prevent the use of Cernox™ (see below). [20]

Platinum

Platinum RTDs are an industry standard. They follow an industry standard curve from 73 K to 873 K with good sensitivity over the whole range. Platinum RTDs can also be

used down to 14 K. Because of their high reproducibility, they are used in many precision metrology applications. Platinum RTDs have limited packaging options, but they are inexpensive and require simple instrumentation. They are widely used in cryogenic applications at liquid nitrogen temperatures or higher. [20]

Rhodium-Iron

Rhodium-Iron temperature sensors can be used over a wide temperature range, and are resistant to ionizing radiation. Wirewound capsule versions (RF-800) have excellent stability and are widely used as secondary temperature standards by many national standards laboratories. Thin-film Rhodium-Iron sensors have various packaging options, including the SD package and bare chip. They require similar instrumentation as a Platinum RTDs, and are used in applications when packaging, size, and temperature range prevent the use of Platinum or Cernox™ sensors. [20]

Cernox™

Cernox™ sensors can be used from 100 mK to 420 K with good sensitivity over the whole range. They have a low magnetoresistance, and are the best choice for applications with magnetic fields up to 30 T (for temperatures greater than 2 K). Cernox™ are resistant to ionizing radiation, and are available in robust mounting packages and probes. Because of their versatility, they are used in a wide variety of cryogenic applications, such as particle accelerators, space satellites, MRI systems, cryogenic systems, and research science. [20]

Germanium

Germanium RTDs have the highest accuracy, reproducibility, and sensitivity from 0.05 K to 100 K. They are resistant to ionizing radiation, but are not recommended for use in magnetic fields. Germanium RTDs are used mostly in research settings when the best accuracy and sensitivity are required. Germanium and Ruthenium Oxide are the only two cryogenic temperature sensors that can be used below 100 mK. [20]

Ruthenium Oxide (Rox™)

Ruthenium Oxide RTDs can be used to below 50 mK. Their unique advantages are that they have a low magnetoresistance and follow a standard curve. Their upper temperature range is limited to 40 K, and Cernox™ are better in magnetic fields above 2 K. Ruthenium Oxide sensors are used for applications that require a standard curve in magnetic fields, such as MRI systems. Along with Germanium, they are the only cryogenic temperature sensors that can be used below 100 mK. [20]

Thermocouples

Thermocouples can be used over an extremely wide range and in harsh environmental conditions, and follow a standard response curve. Less accurate than other cryogenic temperature sensors, special techniques must be employed when using thermocouples to approach temperature accuracies of 1%. Thermocouples are used for their small size, extremely wide temperature range (exceeding high temperature limits of Platinum RTDs), and simple temperature measurement methodology. [20]

Capacitance

Capacitance sensors are ideally suited for use as temperature control sensors in strong magnetic fields because they exhibit virtually no magnetic field dependence. Small variations in the capacitance/temperature curves occur upon thermal cycling. It is recommended that temperature in zero field be measured with another cryogenic temperature sensor, and that the capacitance sensor be employed as a control element only. [20]

Cryogenic sensors using optical fibers

Optical fiber temperature sensors are relatively new to the market when compared with the previous sensors but are gaining importance due to their natural immunity to electromagnetic radiation. As superconducting devices gain more and more in the world of science and technology the demand for sensors capable of working under the harsh conditions needed for superconductivity increases. Based on this demand several technologies have been appearing using optical fibers as sensing elements.

Long period gratings

Fiber optic long period gratings (LPGs) exhibit a number of unique features which make them attractive candidates for in-line filtering applications in telecommunications and for application as sensor elements. A LPG consists of a periodic modulation of the refractive index of the core of an optical fiber. The period of the modulation is typically in the range of 10–1000 μm. The correspondingly small grating wave vector promotes

coupling between co-propagating modes of the optical fiber. In the case of single-mode fiber, the coupling takes place between the guided mode and co-propagating cladding modes. Efficient coupling is thus possible to just a subset of the cladding modes. As the cladding modes suffer from high attenuation, the transmission spectrum of an optical fiber containing an LPG contains a number of attenuation bands, each corresponding to coupling to a different cladding mode [21].

The phase matching wavelengths are governed by the expression:

$$\lambda = [n_{eff}(\lambda) - n_{i\,cl}(\lambda)]\tau \quad (1)$$

Where $n_{eff}(\lambda)$ is the effective refractive index of the propagating core mode at wavelength λ, $n_{i\,cl}(\lambda)$ is the refractive index of the i th cladding mode and τ is the period of the LPG.

Environmental parameters that differentially change the effective indices of the modes of the core and cladding, or that change the period of the LPG, result in a shift in the central wavelengths of the attenuation bands, facilitating the development of sensor systems, or tuneable filters. The sensitivity of LPGs to environmental parameters is influenced by the period of the LPG, by the order of the cladding mode to which coupling takes place and by the composition of the optical fiber. This combination of influences allows the fabrication of LPGs that have a range of responses to a particular measurand — a single LPG may have attenuation bands that have a positive sensitivity to a measurand, others that are insensitive to the measurand and others with a negative sensitivity.

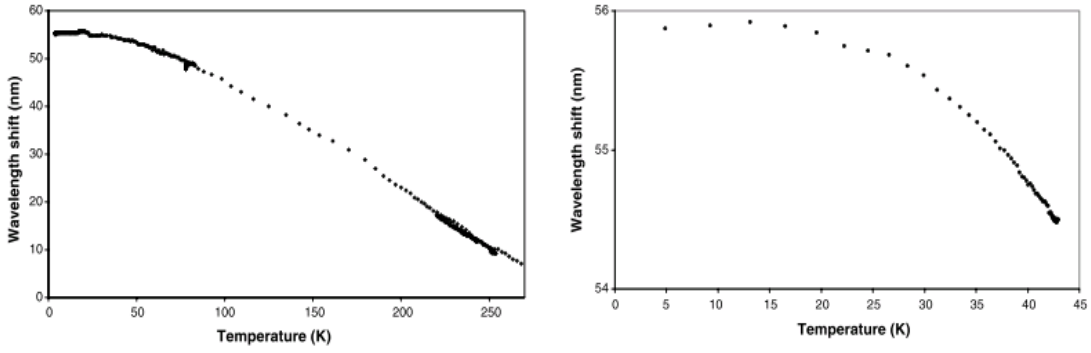

Figure 2 Temperature response of the LPG recorded while cooling the cryostat from 280 to 4.2 K. [21]

The temperature response of fiber optic LPGs has been extensively studied. An example in shown in Figure 2. LPGs with temperature insensitive attenuation bands have been demonstrated in LPGs with short period (40 μm). LPGs fabricated in standard telecommunications optical fiber exhibit temperature sensitivities in the range 30–100 pm/K, an order of magnitude larger than the temperature sensitivity of FBG sensors. For the fabrication of high resolution temperature sensors, or to create widely tunable filters, a number of techniques for further enhancing the intrinsic sensitivity of LPGs have been reported, including the use of fibers of different compositions and different geometries and the use of polymer coatings [21].

Fiber-optic Fabry-Perot interferometer

Most of the Fabry-Pérot (F-P) optical sensors are constructed using an interferometer whose optical path difference (OPD) changes according to the physical parameter to be measure. The sensor OPD is accurately measured by the signal conditioner of either absolute or relative measurement technologies. Thanks to an appropriate sensor calibration, this OPD is converted into the appropriate unit corresponding to the sensor type to display a comprehensive value to the end-user [22].

Two types of F-P temperature sensors are available commercially, capillary type and refractive index type.

The design of the capillary type temperature sensor is actually very simple, two flat-ended fibers are assembled in a glass capillary tube to form a F-P cavity. But the material of one fiber is selected to have a high coefficient of thermal expansion (CTE). The fiber thermal variation is thus not anymore compensated by the one of the capillary tube. Also, this tube is encapsulated into a capillary tube to prevent that the sensor sensing part could be affected by strain transmitted through the packaging. When temperature increases, the thermally sensitive fiber expands, reducing the F-P cavity length. Thanks to factory calibration, this length variation is translated into a temperature value [22].

Several packaging and thermal ranges are available and could be selected depending on the specific needs of the application. Response time of the sensor will of course depend on the selected packaging, but less than 0.5 second is a typical value for a

packaged sensor and about 1ms for a bare sensor. A typical accuracy for this sensor is 0.3K for a medical temperature range (293K to 358K) and 1K for an industrial temperature range (233K to 573K) [22].

Another type of temperature sensor is also available, which instead of the material thermal expansion, temperature dependent refractive index is rather used to change the OPD of the Fabry-Pérot sensor. A tiny chip of a semiconductor material with high thermal refractive index dependence and two semi-reflective surfaces constituting an F-P cavity is assembled at the tip of the lead optical fiber. This solid compact design is actually the smallest optical fiber temperature sensor available on the market (150 μm square). Its sensitivity is about one order of magnitude lower than the capillary type temperature sensor, but due to its extremely low thermal mass, its response time is better than 5 μs for a bare sensor which makes this sensor extremely interesting for fast temperature changes monitoring or for precise spatial point temperature mapping applications [22].

Fiber-optic thermometer probe using fluorescent decay

This is a device for optically measuring temperatures of cryogenic fluids by analyzing the decay in the luminescence of a doped crystal. The device uses a light source for exciting the crystal, an optical fiber for transporting the light flux emitted by the source to the crystal and for returning to a detection assembly the luminescent light emitted by the crystal as a result. A measurement probe is put in the fluid, where the doped crystal is constituted by one of the crystals from the group comprising strontium fluoride doped with divalent ytterbium, $SrF_2:Yb^{2+}$; and calcium fluoride doped with divalent ytterbium, $CaF_2:Yb^{2+}$.

Temperature measurement by means of photoluminescent crystals and of optical fibers is based on a principle that is well known and that relies on measuring the duration τ of the decay time in luminescent light emission from a crystal luminophore after it has been optically excited by means of a light pulse delivered by a light source such as a xenon lamp or a light emitting diode (LED). Notice that, the decay of the luminescence is of the exponential type $I=I^0 e^{-t/\tau}$ where τ is the decay duration and depends both on the temperature and on the crystal used [23].

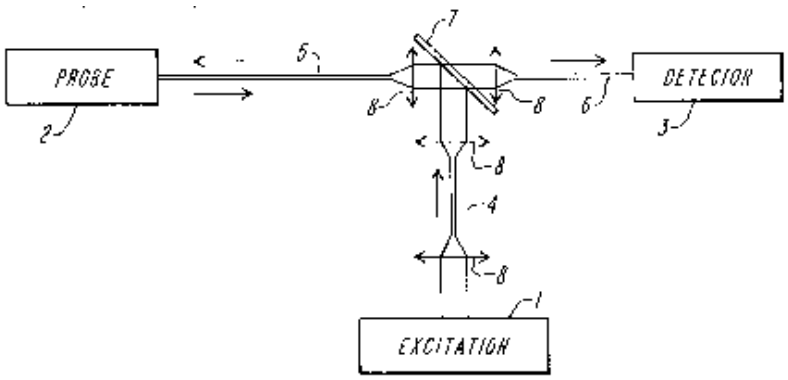

Figure 3 Temperature measurement device using photo-luminescent crystals [23]

Figure 3 is a theoretical diagram of an example of a measurement device that implements the above-mentioned method of measuring temperature. The device comprises firstly an excitation light source 1 which emits light pulses directed to a doped crystal that constitutes the active element of the measurement probe 2, and secondly a luminescence detector 3 which receives the luminescent light emission returned by the doped crystal. Optical fibers 4, 5, and 6 serve to transmit the exciting light pulse to the probe and to return the light emission from the crystal to the detector. Advantageously, in order to limit the number of fibers used by the device, a separator 7 is located at the inlet to a bidirectional measurement fiber 5 that terminates at the probe 2. Where necessary, focusing means 8 enable the inlet and outlet light of the various optical fibers to be focused [23].

Fiber Bragg gratings (FBG)

This work focus only on the study and construction of FBG sensors and their applications as cryogenic temperature sensors.

It was shown experimentally, that the Bragg wavelength of fused silica fibers with Germanium doped core becomes independent on temperature for temperatures below 40 K. This is beneficial for structural health monitoring in cryogenic systems. On the other hand, bare fibers with FBG cannot be used for temperature measurements. [24] To overcome this problem, several solutions were proposed. Fixing the FBG on a substrate that shows a high thermal expansion, for example, PTFE [25], Flint-glass [26], or metals [27] result in a temperature dependence of several pm/K. Alternatively,

metal-coating [17] of the fibers also lead to a measurable temperature dependence of the Bragg wavelength. Also results on the influence of ORMOCER polymer coatings on the temperature dependence of FBG were presented in [28].

In this work metal coated FBGs are the main focus, Figure 4 shows the sensitivities of several FBG sensors with different metal coatings and deposition methods comparing them with a bare grating.

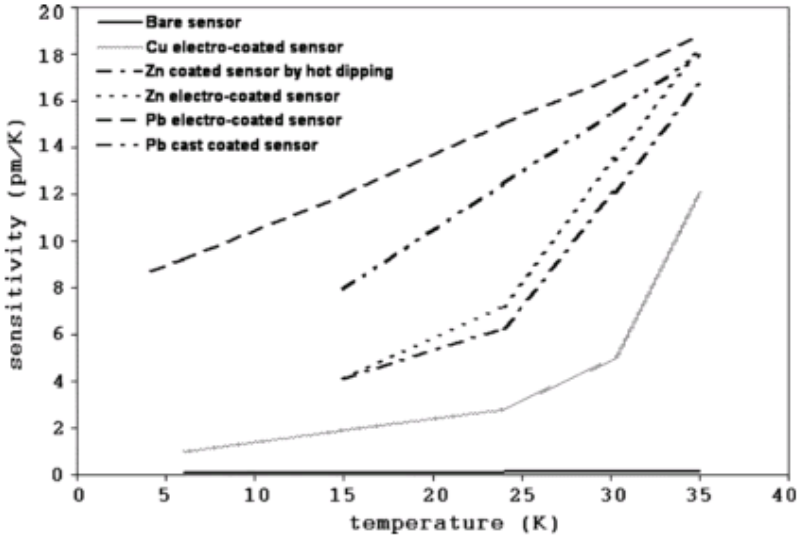

Figure 4 Sensitivities of FBG sensors with and without recoating. [19]

Working principle of a Bragg sensor

Bragg law

When light from a broad band source illuminates the FBG, the wavelength λ_B of the Bragg reflected peak can be expressed as [29]:

$$\lambda_B = 2\eta_{eff}\Lambda \quad (1)$$

Where η_{eff} is the effective refractive index of the FBG and Λ is its period.

For a bare FBG, the shift of center wavelength λ_B caused by the variation of ΔT can be expressed as [30]:

$$\frac{\Delta\lambda_B}{\lambda_B} = (\alpha + \xi)\Delta T = K_T.\Delta T \quad (2)$$

Where α is the thermal expansion coefficient of the fiber, $\xi = \frac{1}{\eta eff}\frac{d\eta eff}{dT}$ and K_T is the temperature sensitivity coefficient of the bare FBG.

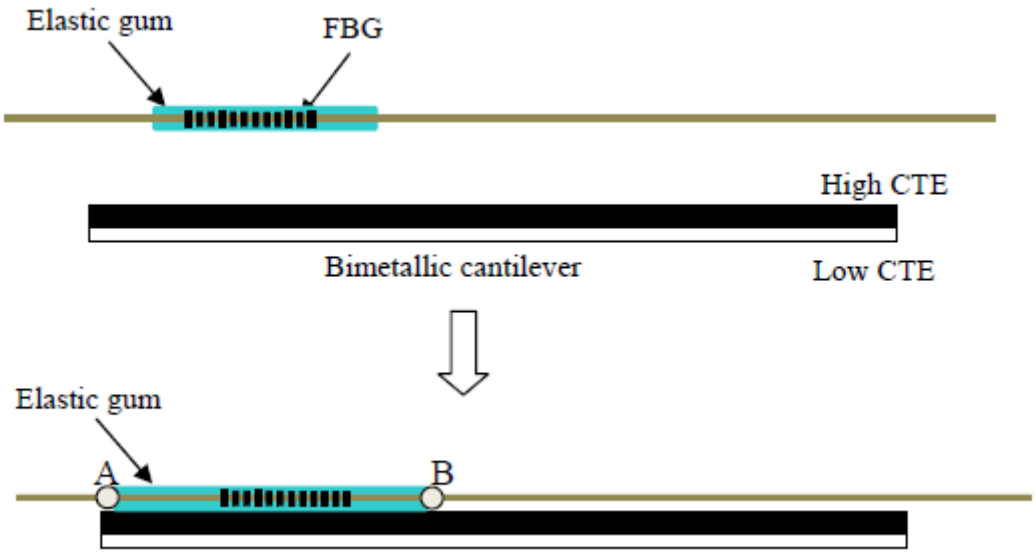

Figure 5 Principle of how FBG sensor sensitivity can be improved [8]

When the bare FBG is attached to a substrate whose thermal expansion coefficient is different from that of the fiber as shown in Figure 5, the shift of the FBG center wavelength with the variation of temperature can be rewritten as:

$$\frac{\Delta\lambda_B}{\lambda_B} = (\alpha + \xi + (1 - p_e)(\alpha_{sub} - \alpha))\Delta T \quad (3)$$

$$\frac{\Delta\lambda_B}{\lambda_B} = (K_T + (\alpha_{sub} - \alpha)K_\varepsilon)\Delta T \quad (4)$$

Were α_{sub} is the thermal expansion coefficient of the substrate material, $K_e = 1 - p_e$is the train-tunning coeffitient, and p_e is the effective photoelastic coeffitient. For a conventional fiber, α≈0.55x10^{-6}/ºC , ξ≈7x10^{-6}/ºC and p_e≈0.22 [8].

If the FBG is bonded along the center of the bimetallic strip, whose expansion coefficient is larger than that of the other, the difference in thermal expansion coefficients of the materials lead to the bending of the strip, further contributing to the shift of the center wavelength of the FBG. Therefore, Eq. (4) should be rewritten as [31]:

$$\frac{\Delta\lambda_B}{\lambda_B} = [K_T + (\alpha_{sub} - \alpha)K_\varepsilon + \alpha K_e(\alpha_{sub} - \alpha_1)\,]\Delta T \quad (5)$$

$$\frac{\Delta\lambda_B}{\lambda_B} = [K_T + (\alpha_{sub} - \alpha)K_\varepsilon + K]\Delta T \quad (6)$$

Where $K = \alpha K_e(\alpha_{sub} - \alpha_1)$ is the enhancement in temperature sensitivity coefficient that results from the strain of the bimetallic strips, $\alpha = [L\,Bh^2E_lE_{sub}] / \{4I[(E_l + E_{sub})^2 + 12E_lE_{sub}]\}$ where E, L, B, h, I and α are young's modulus, length, width, thickness, moment of inertia, and thermal expansion coefficient, respectively. Subscript "*l*" indicates the sheet whose expansion coefficient is smaller, and subscript "*sub*" indicates the sheet whose expansion coefficient is larger. To increase K, the difference in the expansion coefficients of the strips should be increased.

Behavior of a Bragg sensor at cryogenic temperatures

When FBGs are written in optical fiber without coating, the temperature sensitivity of the sensor is governed by equation (2). When placed at cryogenic temperatures, the fibers undergo a great compression becoming an extremely compact structure. This increased density translates into an increase of the effective refractive index, which implies a decrease of ξ and consequently a decrease in sensitivity. When the structure reaches its density limit the sensitivity in the sensor's grating is lost.

How to improve the performance of a Bragg sensor at cryogenic temperatures

Fiber Bragg grating recoating

The FBG sensors use, as discussed above, the shift of the reflected wavelength λ_B by the grating as a parameter of temperature measurement, as can be seen from equation (5). There is no doubt that the coefficient of thermal expansion of the substrate used for coating plays a major role in the sensitivity of this type of sensor. It's the main priority when choosing the material and/or type of substrate. In Figures 6 to 9 can observe the variation with temperature of the length $10^5\frac{\Delta L}{L} = 10^5\frac{L_{293}-L_T}{L_{293}}$, in parts per million of a number of materials and found that different elements show different thermal dependencies on the coefficients of thermal expansion, $\mathrm{CTE} = \frac{10^5}{L_{293}}\frac{dL}{dT}$, and only some have measurable variations at very low temperatures. However, combination of elements and their new structures can result in materials with higher CTE value in the limit of low temperatures.

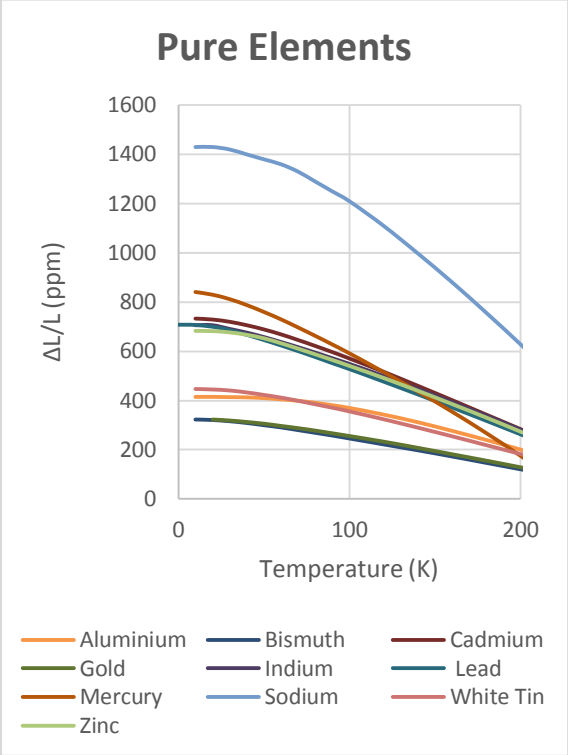

Figure 6 Plot of length variation with temperature of elements metals

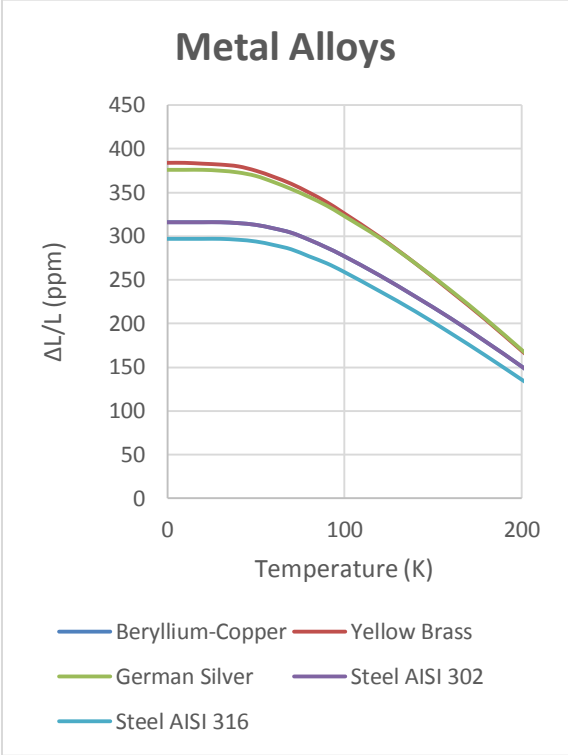

Figure 7 Plot of length variation with temperature of several metallic alloys

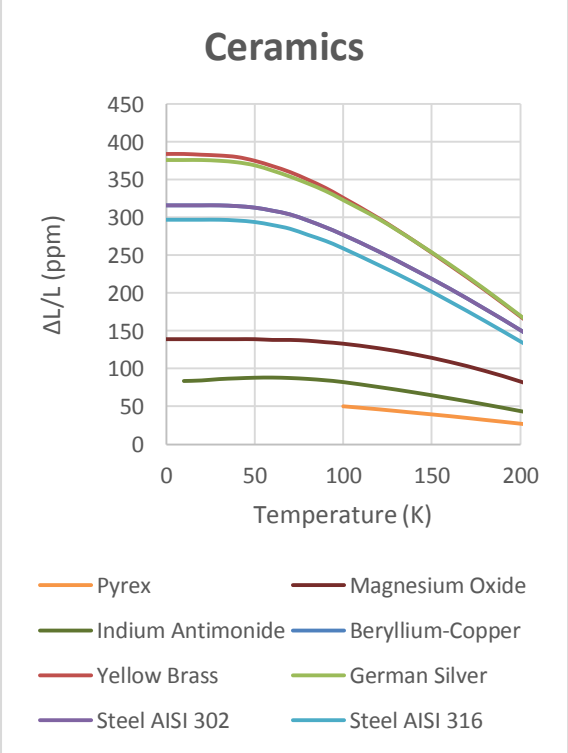

Figure 8 Plot of length variation with temperature of several ceramics

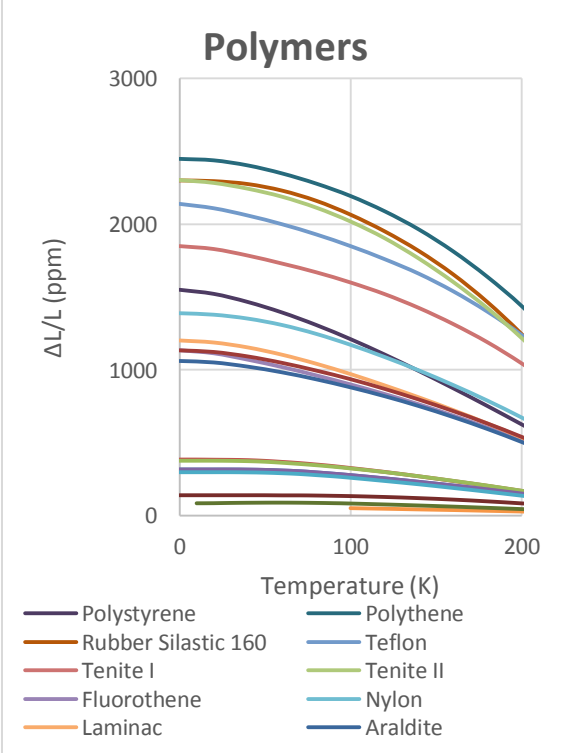

Figure 9 Plot of length variation with temperature of several polymers

There are also studies of materials with Negative Thermal Expansion (NTE) in which occurs a physicochemical process where the material contract upon heating rather than expanding as most materials do. Materials which undergo this unusual process have a range of potential engineering, photonic, electronic, and structural applications.

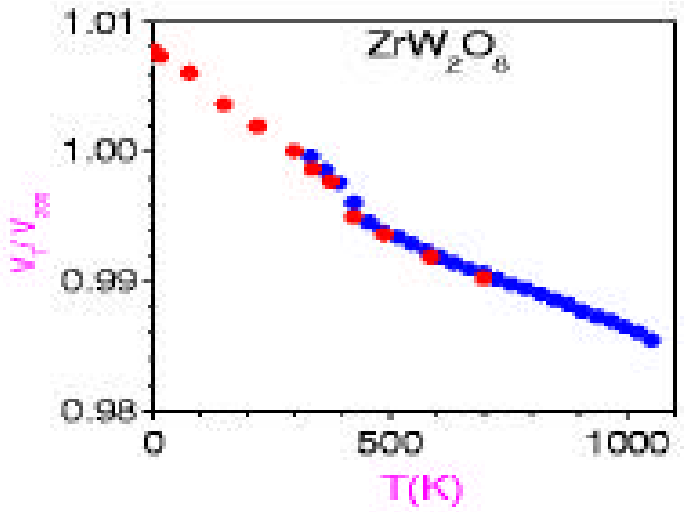

Figure 10 Plot of volume (relative to room temperature volume) expansion vs temperature for ZrW_2O_8 [35]

Perhaps one of the most studied materials to exhibit negative thermal expansion is Cubic Zirconium Tungstate (ZrW_2O_8). This compound contracts continuously over a temperature range of 0.3 to 1050 K (at higher temperatures the material decomposes) [32]. This exotic behavior can be seen in Figure 10 were the relative volume variation is plotted [35]. Other materials that exhibit this behavior include: other members of the AM_2O_8 family of materials (where A = Zr or Hf, M = Mo or W) and ZrV_2O_7. $A_2(MO_4)_3$ also is an example of controllable negative thermal expansion.

Quartz and a number of zeolites also show NTE over certain temperature ranges [33]. Fairly pure silicon has a negative coefficient of thermal expansion for temperatures between about 18 K and 120 K [34]. Cubic Scandium trifluoride has this property which is explained by the quartic oscillation of the fluoride ions. The energy stored in the bending strain of the fluoride ion is proportional to the fourth power of the displacement angle, unlike most other materials where it is proportional to the square of the displacement. A fluorine atom is bounded to two scandium atoms, and as temperature increases the fluorine oscillates more perpendicularly to its bonds. This draws the scandium atoms together throughout the material and it contracts. ScF_3 exhibits this property from 10K to 1100K above which it shows the normal positive thermal expansion.

However, the CTE is not the only factor to be considered, the Young's modulus, E, which is related to the tension exerted on the fiber substrate, is also a crucial factor in the choice of substrate since this will control the expansion of the system establishes dominance over the fiber. When selecting the most suitable materials attention will be given those with higher values of CTE and E.

Coating materials

The coating technique is the main technique approached in this theses being the main focus of the research work. Although for materials where this technique was not applicable a substrate adhesion technique was used.

What is important in a coating material?

Coefficient of thermal expansion (CTE)

The Coefficient of Thermal Expansion is the coating material's most important characteristic. In order to obtain sensitivity at really low temperatures the coating material must still present expansion/contraction at those temperatures. If that doesn't happen in the temperature range of interest then that material should be discarded as a coating.

The Negative Thermal Expansion Coefficient appears in a small group of materials, meaning that instead of compressing with temperature decrease they expand. These materials were to the authors knowledge never tested as a coating for FBG sensors and could present very interesting results, once they should reach a maximum of expansion at 0K.

Young's modulus (E)

The Young's Modulus is the second most important characteristic of the material, because even if it has high CTE if still need to have enough strength to overpower the

bare grating in its own expansion behavior. If this wouldn't happen the sensor would have a negligible improvement when compared to the bare grating.

Adhesion

Adhesion is the final parameter of extreme importance, for even if the two parameters above are met and the coating shows poor adhesion to the grating its impact on the sensitivity would be reduced and could cause the improved sensitivity disappearance after a few cycles. If a coating material with good CTE and E shows poor adhesion to the grating a buffer layer should be used between then. This buffer should have reduced dimensions when compared to the fiber's diameter and coating while presenting good adhesion between both.

Coating techniques

Sputtering

Sputtering process involves ejecting a material from a “target” onto a “substrate” in a vacuum chamber. This effect is caused by the bombardment of the target by ionized gas which often is an inert gas such as argon. An important advantage of sputtering is that even materials with very high melting points are easily sputtered while evaporation of these materials in a resistance evaporator or Knudsen cell is difficult and problematic

Electron beam deposition (EBD)

Electron Beam Evaporation (commonly referred to as E-beam Evaporation) is a process in which a target material is bombarded with an electron beam given off by a tungsten filament under vacuum. The electron beam causes atoms from the source material to evaporate into the gaseous phase. These atoms then deposit in the substrate, coating everything in the vacuum chamber (within line of sight) with a thin layer of the anode material. A clear advantage of this process is it permits direct transfer of energy to the source material during heating and very efficient in depositing pure evaporated material to substrate. Also, the deposition rate in this process can be as low as 1 nm per minute to as high as few micrometers per minute. The material utilization efficiency is high relative to other methods and the process offers structural and morphological control of films. Additionally, coating uniformity and precise layer monitoring techniques are also some advantages with this process.

Electrodeposition

Electrodeposition is a process that uses electrical current to reduce dissolved metal cations so that they form a coherent metal coating on an electrode. The term is also used for electrical oxidation of anions onto a solid substrate, as in the formation silver chloride on silver wire to make silver/silver-chloride electrodes. Electroplating is primarily used to change the surface properties of an object (e.g. abrasion and wear resistance, corrosion protection, lubricity, aesthetic qualities, etc.), but may also be used to build up thickness on undersized parts or to form objects by electroforming.

The process used in electroplating is called electrodeposition. It is analogous to a galvanic cell acting in reverse. The part to be plated is the cathode of the circuit. In one technique, the anode is made of the metal to be plated on the part. Both components are immersed in a solution called an electrolyte containing one or more dissolved metal salts as well as other ions that permit the flow of electricity. A power

supply supplies a current to the anode, oxidizing the metal atoms that comprise it and allowing them to dissolve in the solution. At the cathode, the dissolved metal ions in the electrolyte solution are reduced at the interface between the solution and the cathode, such that they "plate out" onto the cathode. The rate at which the anode is dissolved is equal to the rate at which the cathode is plated. In this manner, the ions in the electrolyte bath are continuously replenished by the anode.

Other electroplating processes may use a non-inert anode such as Platinum or Carbon. In these techniques, ions of the metal to be plated must be periodically replenished in the bath as they are drawn out of the solution.

Dip – Coating

In a dip-coating process, a substrate is dipped into a liquid coating solution and then is withdrawn from the solution at a controlled speed. Coating thickness generally increases with faster withdrawal speed. The thickness is determined by the balance of forces at the stagnation point on the liquid surface. A faster withdrawal speed pulls more fluid up onto the surface of the substrate before it has time to flow back down into the solution. The thickness is primarily affected by fluid viscosity, fluid density, and surface tension.

Dip-coating, while excellent for producing high-quality, uniform coatings, requires precise control and a clean environment. The applied coating may remain wet for several minutes until the solvent evaporates. This process can be accelerated by heated drying. In addition, the coating may be cured by a variety of means including conventional thermal, UV, or IR techniques depending on the coating solution formulation. Once a layer is cured, another layer may be applied on top of it with another dip-coating / curing process.

Casting

Casting is a manufacturing process by which a liquid material is usually poured into a mold, which contains a hollow cavity of the desired shape, and then allowed to solidify. The solidified part is also known as a casting, which is ejected or broken out of the mold to complete the process. Casting materials are usually metals or various cold setting materials that cure after mixing two or more components together; examples

are epoxy, concrete, plaster and clay. Casting is most often used for making complex shapes that would be otherwise difficult or uneconomical to make by other methods.

Process production and measurements

After the study of the state of the art related to the construction of FBG temperature sensor and deciding that the focus of this work would be on recoated FBGs a few materials were chosen. An analysis of figure 4 suggested Lead(Pb), Indium(In), and Mercury(Hg) as top candidates for recoating materials due to their high CTE, of these Mercury showed the highest and so due to ease of access it was the first one to be tested.

Mercury tests

In experiments with mercury coated sensors there were added difficulties in testing, since this metal is liquid at room temperature. The fiber coating was tested with the immersion technique on the material without the use of any cryogenic adhesive.

A1 A2 A3

Figure 11- A1) Capillary hole filled with mercury where the fiber was immersed; A2) a liquid nitrogen bath where the sensor block is cooled to 77K; A3) sensor block after thermal bath in which the variation in wavelength is measured with the slow rise of temperature.

As can be seen in the images a1 to a3 on Figure 11, a copper cylinder with cylindrical capillary holes was used, one of which was filled with mercury at room temperature using a syringe. The fiber was inserted into the filed hole with the sensor immersed in the mercury, the entire assembly was placed in an aluminum block and subsequently cooled in liquid nitrogen. These blocks of great dimensions compared with the optical fiber were used to protect the fiber from sudden changes in temperature allowing a

lower warming rate greatly improving the accuracy in the measurements and the amount of data acquired.

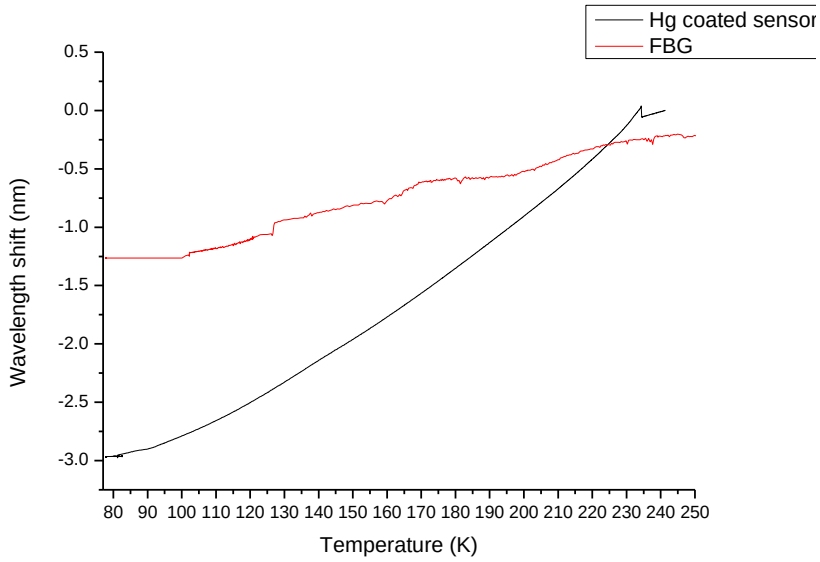

Figure 12- Wavelength shift of the sensor immersed in mercury, during warm up, compared with a regular FBG with no coating.

In Figure 12 it's possible to verify the change in wavelength of the sensor with temperature rise, when the block is removed from the liquid nitrogen after reaching thermal equilibrium. However, the wavelength shift does not correspond to that expected for this material. This is due to the fact that mercury at room temperature has a really high surface tension, although the fiber has been kept inside the hole the Mercury pushes it to the surface of contact between himself and the copper block. It was therefore impossible to determine the real effect of the mercury in the fiber, since the tension applied to the fiber is due not only to mercury, but also to copper.

A new test was designed to determine the maximum wavelength shift of this sensor. The fiber was dipped in a cylindrical cavity much greater than it's radius (approximately 15mm diameter), and fully filled with mercury. There was some difficulty introducing the fiber into the liquid mercury due to the surface tension that created a deflection of the flexible fiber. When able to stabilize the fiber immersed in mercury, the container was immersed in liquid nitrogen until they reach thermal equilibrium. At this point although the fiber was completely immersed on mercury it was impossible to determine if there was any bending of the grating, a grating without any coating was also used and inserted in the setup for comparison purposes.

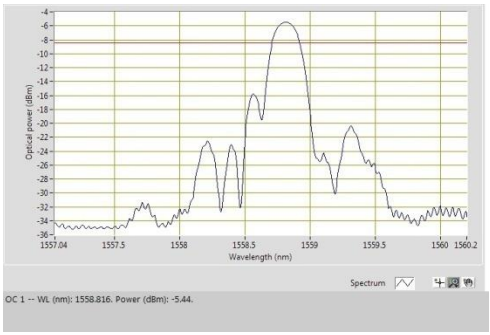

Figure 13 FBG spectrum at room temperature with Mercury immersion.

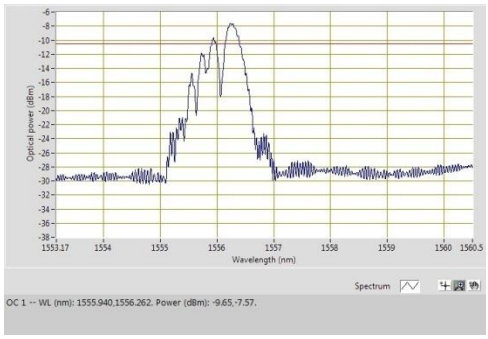

Figure 14 FBG spectrum at 78K for the sensor not immersed in Mercury.

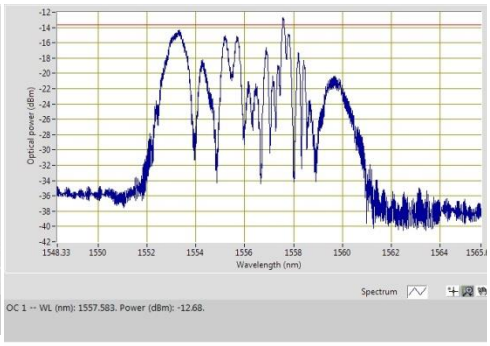

Figure 15 FBG spectrum at 78K for the sensor immersed in Mercury

The spectra in Figures 13 to 15 represent, respectively, the reflection spectra for both fibers, immersed and not immersed at room temperature and after lowering the temperature to 78 K . It can be seen that at the temperature of 78 K, the reflected spectrum does not show a well-defined maximum, but rather a set of maximum and a correct precise reading cannot be made of the wavelength shift. In order to make the measurement the as reliable as possible, only the data measured from the peak that remains present during all measurement is taken in account.

The series of peaks seen in Figure 15 are due to the fact that the cooling and solidification of mercury was not homogeneous along the length of the sensor, curing a gradient of stresses exerted on the grating by the mercury, which changes the effective index in each sensor section.

Also the values obtained for the wavelength shift were not reliable once it was impossible to determine if the grating was bent and if with the Liquid-Solid phase transition that bent was increased.

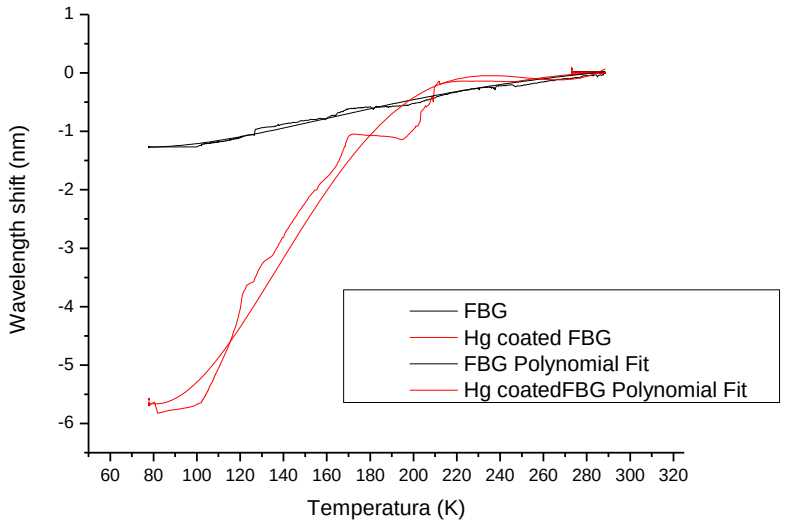

Figure 16 Wavelength shift with temperature of two FBG sensors one with Hg coating.

The wavelength shift during the warm-up was recorded using LabVIEW software for the immersed and not immersed fibers. The observed behavior was then obtained in the chart of Figure 15 where the wavelength shift curve of the grating immersed in mercury does not have the expected behavior like the one illustrated in Figure 12, presenting steps. These steps are due to the fact that some of the peaks seen in Figure 16 overlap with each other at different temperatures for the reasons already described above.

However, and despite the high uncertainty of measurement, it is possible to measure a variation of 5.7 nm between the resonant wavelength at room temperature and at a temperature of 77 K, which is twice the sensitivity obtained in the first test with this element .

When compared at the temperature of 80 K, the wavelength shift of sensors coated with lead described in [17] are more sensitive than the sensors immersed in mercury presenting a shift of 8nm.

This example is interesting academically, because although has a higher CTE at low temperatures than lead, mercury has a much lower Young's modulus, failing to exert enough tension to subject the fiber and causing it to deform as much as itself with temperature decrease.

A compromise has to be made between CTE, Young modulus and Adhesion, so it was decided to re-focus the project on Indium and Lead and other materials would only be considered if they were easy to be obtained and used by the author.

Recoating tests

At this point coating techniques had to be explored for Lead and Indium, and as they are on a solid phase at room temperature techniques like immersion were not applicable. After contacts made with the research group INESC Dr. Luis Coelho was indicated to the author as a researcher experienced in deposition of metals on fibers.

Due to his own previous experience this researcher informed the author that Lead didn't present adhesion to the fibers and the metals with the best adhesion were Chromium (Cr) and Titanium (Ti).

With this information it was decided to do bimetallic film depositions on the gratings, where an internal layer of Chromium or Titanium would serve as buffer improving the adhesion between fiber and external coating. Soft metals like Indium and Lead don't have the necessary Young's modulus to transmit their expansion to the fiber this transmission would be ensured by the buffer layer.

Electron beam deposition (EBD)

This technique was used to do the buffer depositions once it's able to deposit thin films with high homogeneity.

Figure 17 Opened EBD chamber used for thin film deposition of the buffer layers on the FBGs.

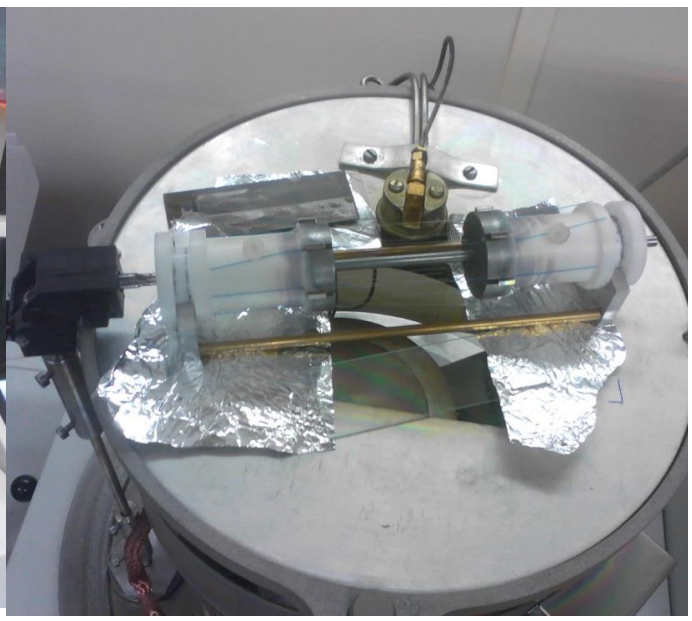

Figure 18 Apparatus that allowed for the homogeneous thin film deposition on multiple fibers.

The films deposited were 100 to 200 nm thick and made of Titanium, Chromium and Nickel. A device designed and created by Dr. Luis Coelho was inserted in the vacuum chamber of the EBD device. This device represented on Figures 17 and 18, allows for the even and simultaneous deposition of materials on six fibers rotating them at a constant speed inside the chamber.

In order to do this deposition the fibers were placed on the rotating device at 6.6 rpm the chamber was put in 10^{-7} vacuum which took around 3 hours, then the deposition started at approximately 0.03 nm/s. Due to the fact that the metals used had high melting points and that the energy dissipated in the form of heat inside the chamber was also high, the deposition had to be paused for around 1hour every time it got too hot. This meant that the device had to be pause after every 30 to 40 minutes witch meant once for to produce a 100 nm film and 3 to 4 times to produce a 200 nm film.

Deposition tests were made on several fibers and on glass substrates in order to test their adhesion. These were cleaned with water, alcohol and acetone on a Quimwipe paper, and then dipped on liquid Nitrogen no pealing of the films was observed.

A Scanning Electron Microscope (SEM) was used on one of these fibers deposited with a 100nm thin film of Chromium.

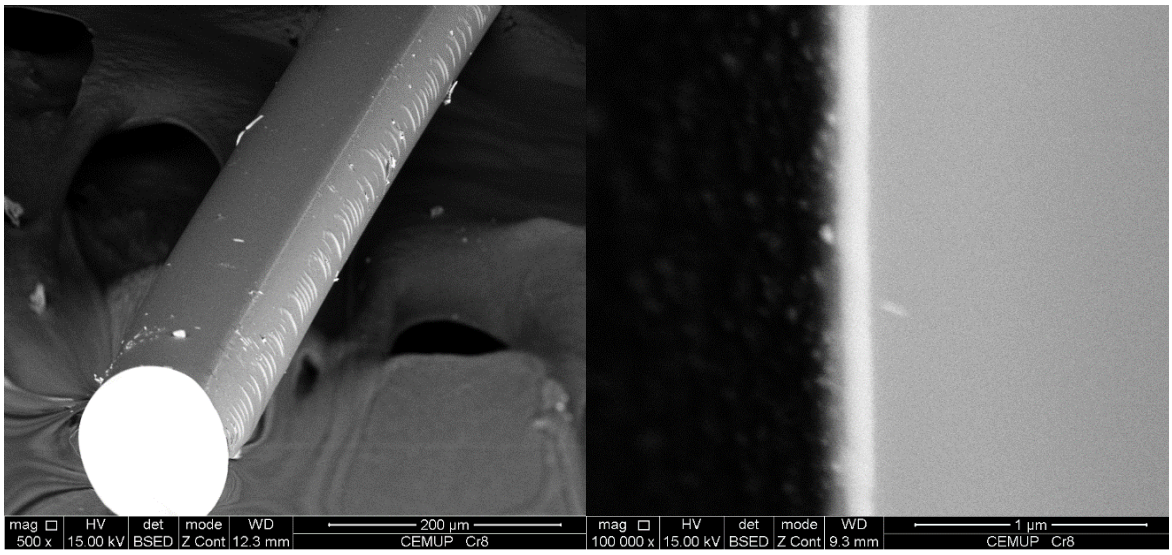

Figure 19 SEM analysis of an optical fiber partialy coated with 100nm Cr thin film

In the SEM images from Figure 19 it is possible to see apart from some debris that the film described above is very homogenous and presents no cracks or pealing. The Chromium thin film on the first image corresponds to the darker part of the fiber being the lighter one an electrodeposition of Nickel that will be described ahead.

The EBD was established to be a very good deposition technique, Titanium and Chromium were proven to have good adhesion to the fiber, and all future work was established on this premise.

Electron Beam Deposition however do not allow for a good deposition of thick films of around 500 microns which was the thickness intended for the outer layers. The fact that this is a Physical Vapor Deposition (PVD) does not allow for all the atoms to be chemically bound together resulting in grains for thicker films. Another disadvantage is that for high thickness this technique is too time and power consuming. Other techniques were considered for this external thick coating.

Sputtering and thermal evaporation

Sputtering and Thermal Evaporation techniques were thought to be used for structural external coating of the FBGs even being PVD resultant and with all the cons that come from it. They would be faster and would be able to deposit thicker films than the EBD, with the cost of higher losses of metal.

However it was found that the available deposition facilities did not possess the capability for even depositions around the fiber and so further tests using these techniques had to be abandoned.

Electrodeposition

Electrodeposition comes referred in most articles on FBG recoating for Temperature measurement like the ones from Dr. Carla Lupi and Dr. Rajini K. Ramalingam as the best deposition technique for this purpose. Allowing for the deposition of films in the hundreds of microns scale were the atoms are chemically bound and the thickness is homogeneous throughout the fiber. Having this in the consideration this technique was a great focus of this project.

Due to material availability and large experience and knowledge possessed the IFIMUP-IN group tests were initiated for the electrodeposition of Nickel on the Chromium and Titanium buffers previously described.

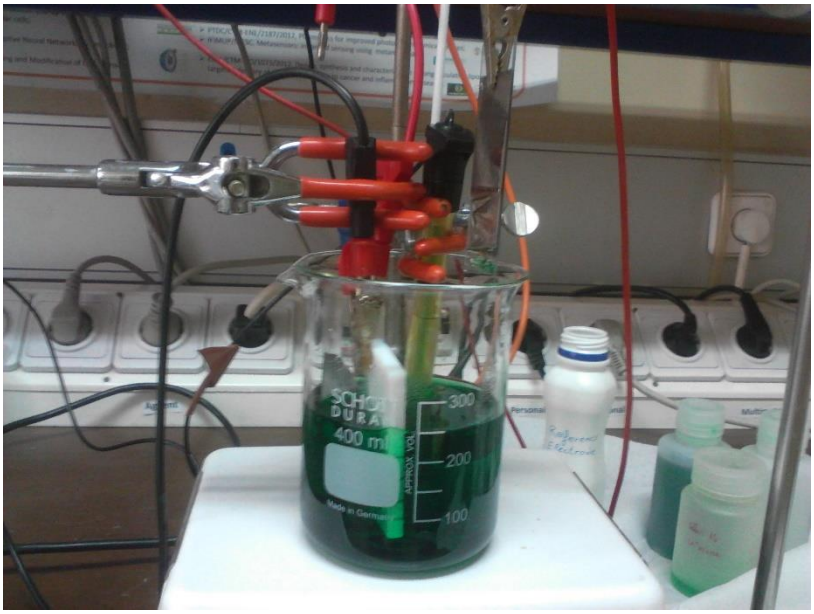

Figure 20 Aparatus used for the Ni electodeposition on a glass substrate with 200nm Cr coating.

In Figure 20 is represented the apparatus used for the electrodeposition tests, a Nickel bath was already available from previous usage. The bath solution was composed by 300g/L of $NiSO_4.6H_2O$ + 45g/L of $NiCl_2.6H_2O$ + 45g/L of H_3BO_3 and was keep at 41ºC during deposition.

With the assistance of Dr. Arlete Apolinário, a researcher at IFIMUP-IN experienced in electrodepositing Nickel on metallic surfaces, tests were conducted in order to find the best Platin electrode shapes, current intensity and metallic contacts.

Only plan electrodes were available that were only ideal for deposition on planar surfaces, so the depositions on the fibers had to be tested using this electrodes that only deposited on one side of the fiber. From these ones one was chosen for his small size and tight Platinum grid once the fiber surface was very small. A cylindrical electrode with a tight Platinum grid would be necessary for an even deposition around the fiber

Tests started by using thing 200nm films of Chromium and Titanium on plan grass substrates. A voltage difference of 1.5V was applied between the electrode and the films and the current was measured for a period of 25 minutes for the Cr film and 7 min for the Ti film. After these periods the Ni films deposited on the Cr film cracked and pealed, and there was no visible Ni film visible over the Ti film. The currents measured were respectively 92 mA and 0,75 mA for Chromium and Titanium substrates.

Figure 21 Ni eletrodeposited on a 200 nm Cr film

Figure 22 Ni eletrodeposited on a 200 nm Ti film

Figure 23 Ni eletrodeposited on a small piece of Ti foil.

As it can be seen from Figures 21 to 23 that the deposition was occurring over the Cr substrate but not over the Ti one that despite the fact that the electric contact was tested prior to the deposition on both cases. There could be a bad adhesion between Ti and Ni so the electrodeposition was tested on a Ti foil for 5 minutes and a current of 60 mA. The result shown on Figure 23 demonstrates that the deposition of Ni over Ti can occur meaning that the thickness of the Ti film used was not enough to allow the necessary current for deposition.

A study was conducted varying the deposition time of Ni over fibers coated with 200 nm of Cr and Ti the electric contacts between the thin films was enhanced by dropping liquid In on the films tip and letting it solidify ensuring that every side of the fiber had electric contact.

The results were that no deposition on the Ti coated fibers was observed, and that all depositions on Cr coated fibers over 30 seconds would peal for the same voltage of 1,5V. The depositions on the Cr coating for 30 seconds seemed homogeneous at the naked eye and was reproducible but there was no idea of its thickness. A SEM and EDS analysis was then made

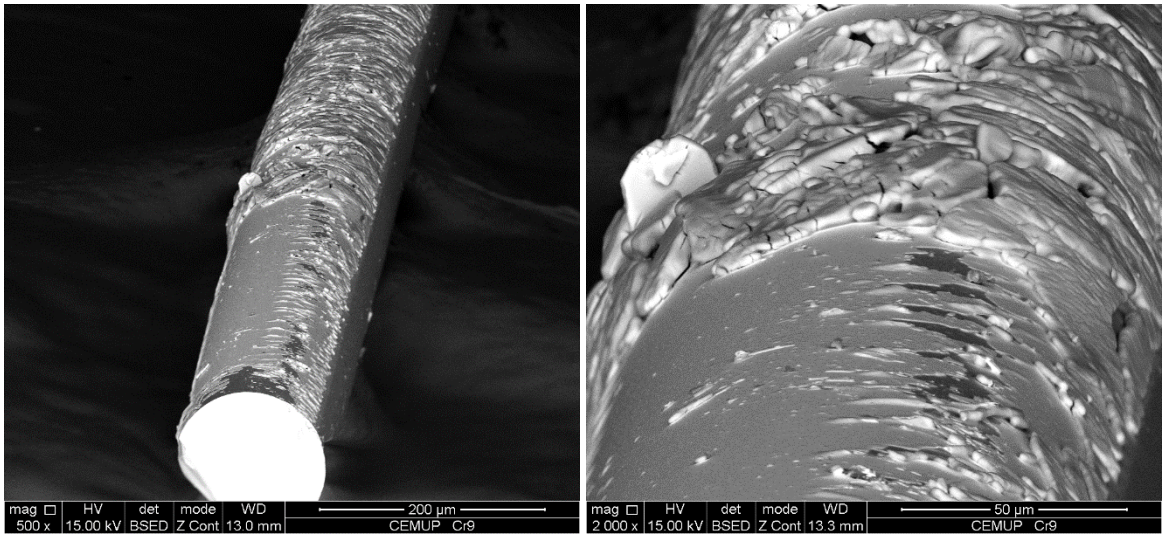

Figure 24 SEM images of a fiber partialy coated with a 200 nm Cr thin film after undergoing eletrodeposition for 30 seconds on that film.

From the images in Figure 24 we can see that the fiber coated with Cr and plated with Nickel that appeared to be homogeneous to the naked eye as in fact not that homogeneous. On the tip of the fiber we see that when this was cut for the SEM analysis most of the Ni was removed there we see and homogeneous of really low width on the rest of the visible fiber it's possible to see grain like structures. This deposition had to be studied in more detail for a better plating of greater width but it was clear that it would be possible with time.

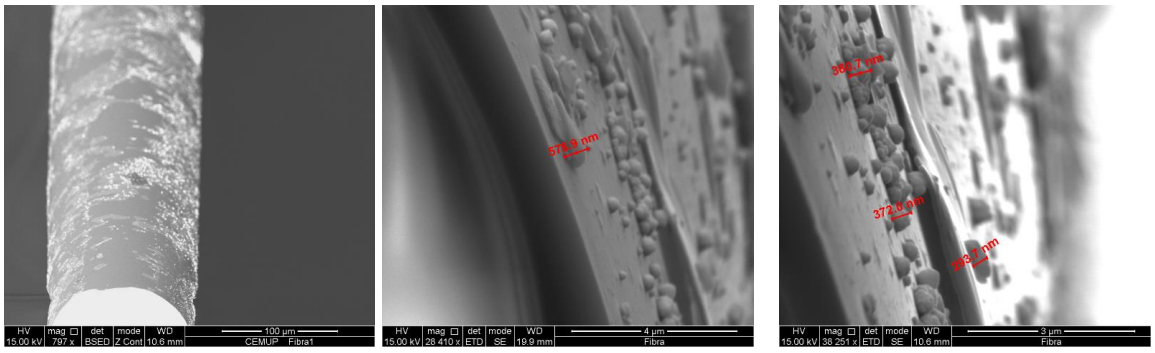

Figure 25 SEM images of a fiber partialy coated with a 200 nm Ti thin film after undergoing eletrodeposition for 7 minuts on that film.

In Figure 25 it's possible to see the Ti coated fiber where there was no visible deposition of Ni except for really small grains to far apart which lead to consider that it might be needed to increase the deposition time. Meanwhile the grains were very similar in size and there were many areas of the fiber with no plating, the plating process was not homogeneous. An EDS test was conducted in order to determine if there was any Ni on the areas that seemed unplated and confirm that there was no peeling of the Ti on those areas.

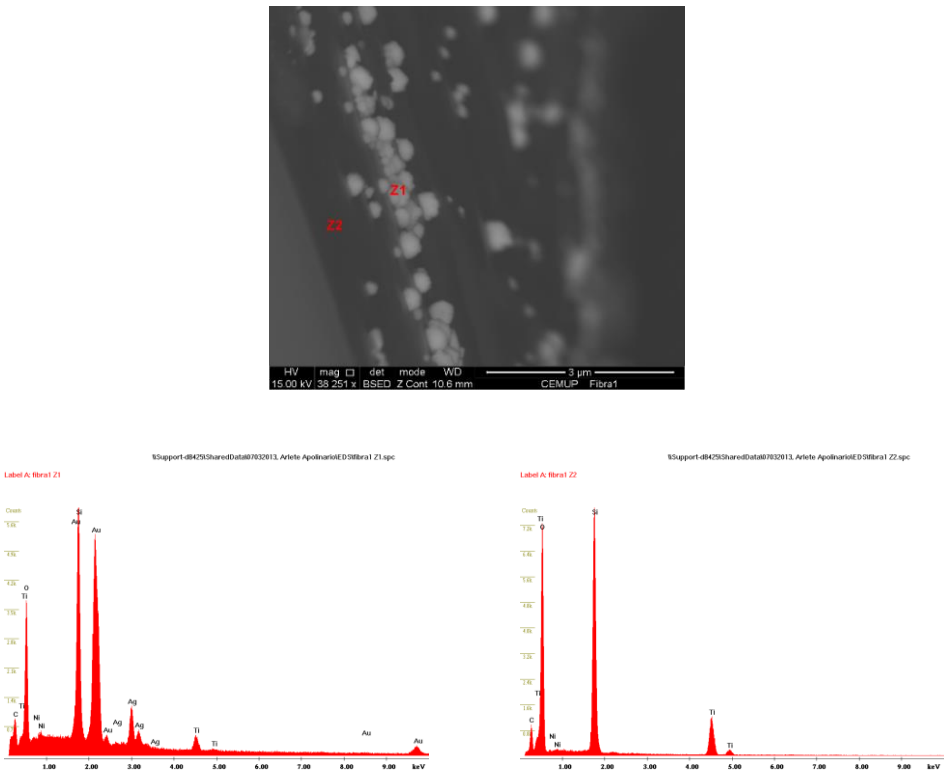

Figure 26 EDS analysis of the small grains deposited on the Ti shown in Figure 25

Images in Figure 26 show the results obtained from the EDS analysis on a plated and on an unplated area. On the plated area there was almost no Ni instead there were high amounts of Gold (Au), an element that should not be there once it is not an integrant part of the plating bath. It was clear that the plating bath was contaminated with Au from previous usage and that this element was the only one being deposited not the Ni.

Analyzing the unplated area it's possible to see that there is also no Ni there, but that the Ti film was still there unpeeled from the fiber by the plating bath.

At this point it was clear that an electrodeposition study of one metal on another was very time consuming. The intention was to deposit not only Ni but mainly In and Pb, that added to the fact that the deposition was occurring on a thin film around a fiber with a very reduced plating would take an even more careful and time consuming study.

The exploration of this technique achieving homogeneous depositions of In and Pb films on Cr and/or Ti with widths that far exceeded the diameter of the fiber, without previous background experience on that particular deposition would take time that would exceed the duration of this work. However to this day it is the author's opinion

that the electrodeposition is the best technique to produce the coatings needed for this FBG temperature sensors, being theoretically the one with higher homogeneity, thickness, atomic bonding and able to deposit any metal.

In order to achieve a working FBG sensor by the end of this project time frame a compromise had to be made at this point for a coating technique that although would not produce the most homogeneous coatings would be able to present results. This coating should have widths way larger than the fiber's diameter to a point where the superficial inhomogeneity could be neglected, and there should be chemical bonding preventing the creation of grains.

Dip-coating and Casting come referred on literature as poor techniques for coating FBGs not only because of their low homogeneity but also because of the temperatures needed in those processes. They had to be considered at this point in order to be able reach the FBG temperature sensor prototype in time.

Dip-coating

This technique was approached not as a despair but because of the melting points of all materials involved. The optical fiber can go up to 873K without any permanent deformation or grating eraser, and the melting points of In and Pb are 429.6K and 600.5K respectively. This means that with a controlled temperature setup the metals could be melted and the fiber dipped inside them.

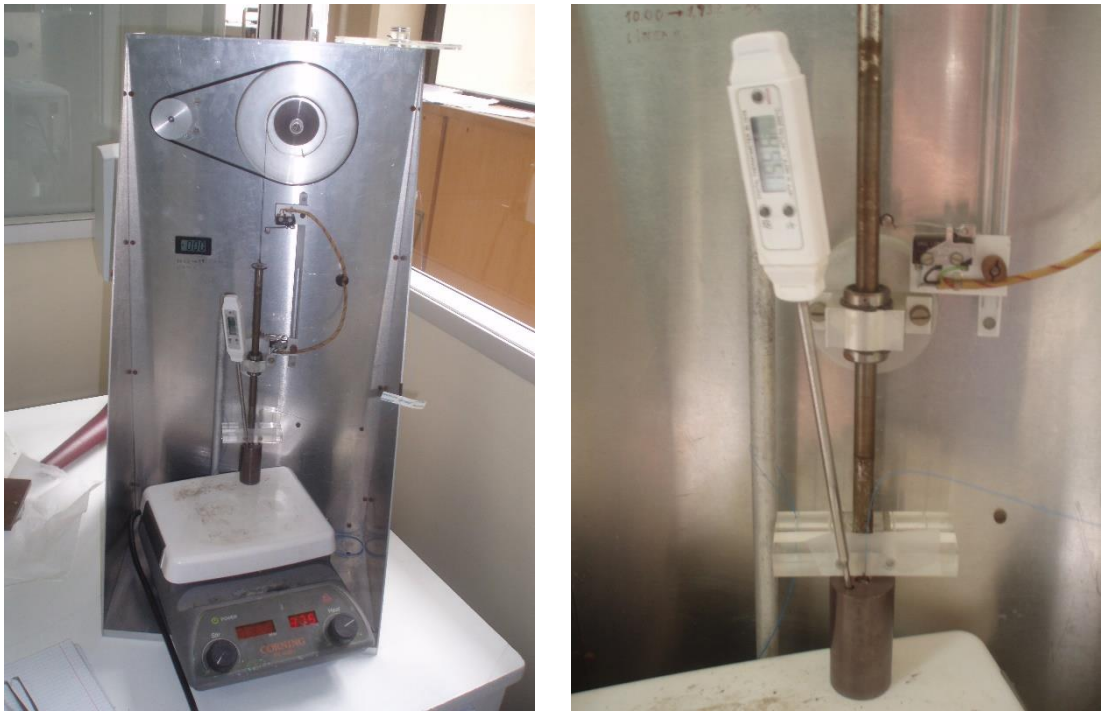

Figure 27 Dip-Coating aparatus used in the coating tests featuring

On the images from Figure 27 is shown the setup used to test the Dip-Coating technique, a heating plate with temperature control able to reach 873K was used to heat a cylindrical copper block with two cylindrical cavities. The central cavity was 6 mm in diameter and 45 mm deep and was used to place a cup filed with the material to be melted, the second one was 3 mm in diameter and 15 mm deep and was used to place a thermocouple with temperature display. A copper block was used due to the thermal conductivity of this material that ensured that there was a better more homogeneous temperature distribution throughout the cup and the metal inside than placing the cup on the heating plate.

Then using a device available at INESC that allowed for a speed controlled vertical movement, the fibers were dipped on the cup containing the melted metal. The fiber was vertically placed on a support existing on this device and after dipped, was removed from the cup at different speeds. The liquid metals, Indium, Tin and Lead were at a temperature as close as their melting points as possible in order to improve viscosity.

Once again and like in the Mercury tests due to the liquid metals surface tension the fibers had the tendency to bend and get pushed to the side of the cup. Unlike a polymer gel deposited by dip-coating where the fiber go in and out the gel in metals a reentrance would only remelt the deposited material removing it, so it could be only removed once at a constant speed.

After many cycles with both materials and both pre-coatings of Cr and Ti the result was always the same the metal would solidify in tiny spheres, being the size and distance between these spheres the only thing that changed. This happened due to the cohesion of the metal itself creating drops of different sizes.

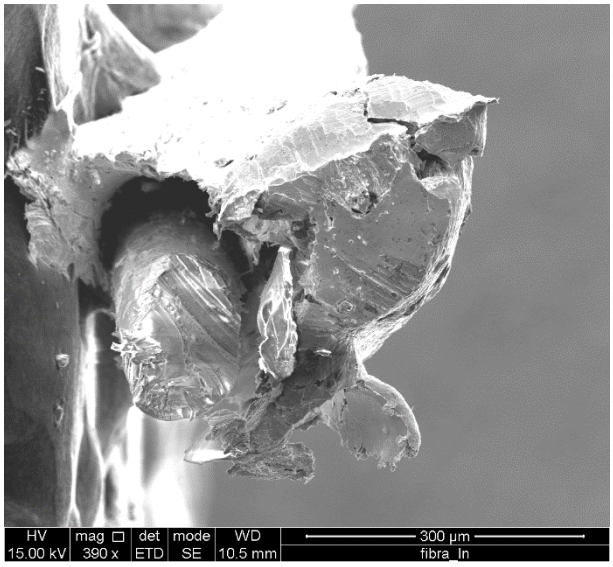

Figure 28 SEM image of the fiber with the best dip-coating deposition to the naked eye.

Figure 28 shows the fiber with the best aspect obtained from the use of dip-coating techniques, the fiber had no pre-coating and In was being deposited. Besides the fact the In was not equally distributed around the fiber it's possible to observe that this metal's adhesion to the fiber is not the best.

Besides the fact that this coating technique proving invalid to this project, the fact that there were no permanent deformation to the fiber and no peeling was observed on the Cr, and Ti films suggested that a casting technique would be applicable for In and Pb.

Casting

Casting comes referred in the literature as a bad coating technique for FBGs due to the usage of high temperatures and low surface homogeneity. Truth is that the elements with the highest CTE like Mercury, Gallium, Indium, Tin and Lead all have also in common low melting temperatures and all below 873K.

This technique was considered a valid alternative since the temperatures required do not affect the fiber or the thin films. Also in order to attenuate the low homogeneity at the sensor's surface the casting mold to be used would have a diameter at least 15 times the diameter of the fiber.

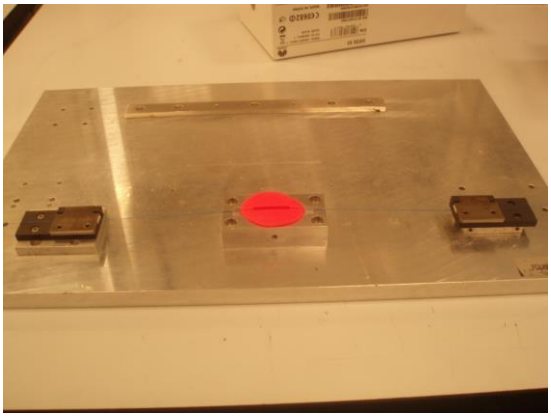

Figure 29 Apparatus used for the sensor construction.

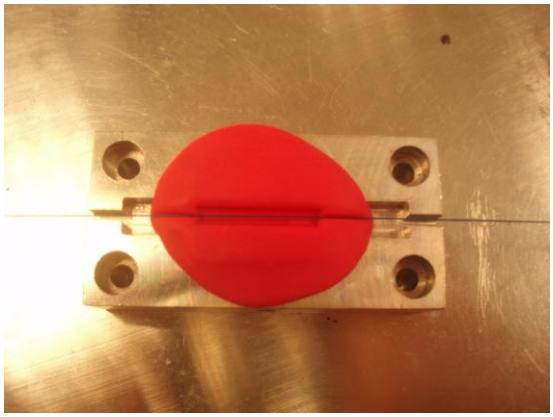

Figure 30 Mold used for the sensor construction.

A mold was made of CERNIT, a thermal insulating polymer easily moldable where the shape of a small cylinder was imprinted, as well as a channel for the optical fiber, in order for it to be centered with the cylinder. Magnetic clamps were used to hold the fiber in place. This apparatus can be observed in Figures 29 and 30. The CERNIT mold underwent a 30 minutes annealing at 393K where it lost its malleability and became rigid.

An optical fiber with a FBG was placed on the mold ensuring that the grating was inside the cylindrical impression. The gratings used were previously recoated with 200nm of Titanium or Chromium, using Ebeam deposition. Using temperature controlled soldering iron small pieces of the metal in study were melted until the cavity was filed. After ensuring the grating was inside the metal the assembly was left to cool. This cavity was approximately 15mm long and 2.5mm in diameter.

During this process the fiber containing the FBG was connected to a BraggMETER and the spectrum was monitored for changes which helped ensure that there were no tensions on the grating before it was left to cool. It was not possible to ensure this in every case.

The spectra and the wavelength shift were monitored and recorded using a BraggMETER and LabVIEW software. The spectrum of each grating was recorded at room temperature and at 77K, this temperature was achieved using liquid Nitrogen. The temperature was measured with a Fluke 1502A Thermometer Readout and recorded with the same LabVIEW software.

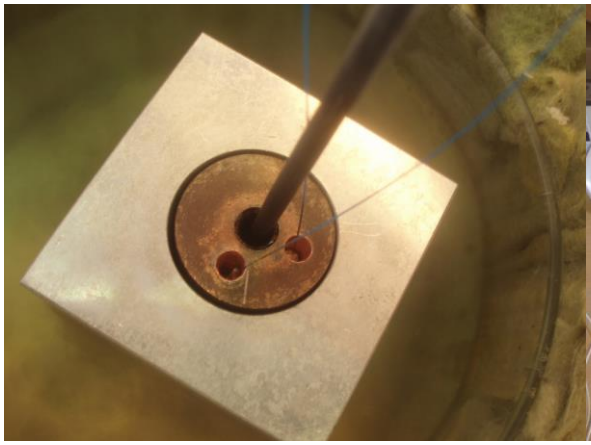

Figure 31- Test block containing 2 sensors and the thermometer.

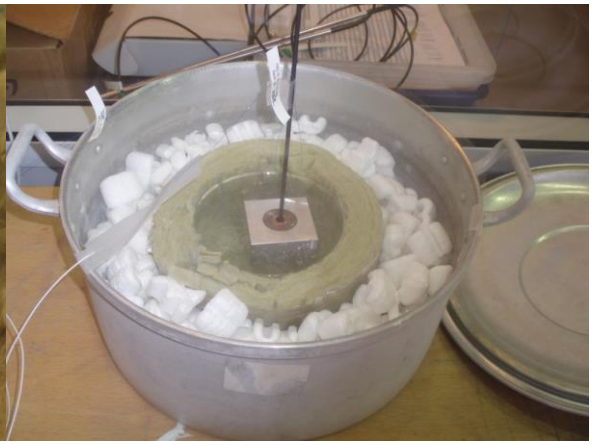

Figure 32- Cryogenic bath using liquid Nitrogen.

The sensors and the thermometer were inserted into a Copper cylinder which was inserted into a block of Aluminum as can be seen in Figure 31. This was made in order to avoid fast temperature variations due to these materials heat capacity. This entire block was then placed in a glass cuvette which was thermal isolated with Styrofoam and then covered by liquid Nitrogen as can be seen in Figure 32.

Two preliminary tests were conducted as described above, the first one using Ti as a buffer and the second Cr. Coatings of Tin and Indium were used, at this point testing a Lead coating was not an option because its melting temperature was above the maximum operation temperature of CERNIT.

First Test

On the first test conducted the Titanium buffered sensors were used, being one recoated with Indium and the other with a Tin alloy. The test was conducted as described until the entire block was at the temperature of 77K. At this point the block was removed from the bath and left at room temperature to heat up-to room temperature.

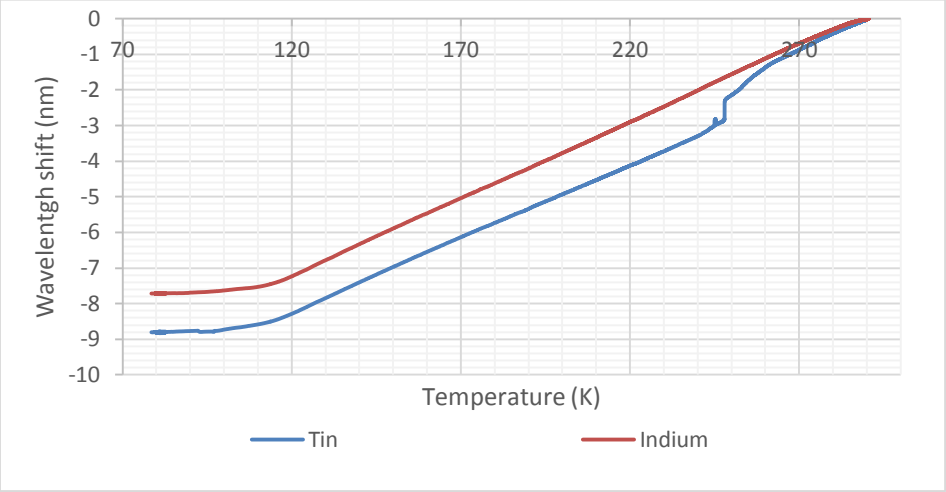

Figure 33- Wavelength shift with temperature of FBGs with 200 nm Titanium buffers one with recoating of Indium and the other a Tin alloy.

The wavelength shift was measured as the temperature increased to room temperature as can be seen in Figure 33.

There was a linear behavior for temperatures over 113K in the case of the Tin sensor can be seen a jump in the wavelength shift at 143K this occurred due to the appearance of new maxima in the spectrum during the heating process. The values obtained for the Tin sensor at the room temperature are the real ones that correspond to the maximum measured when the sensor was built.

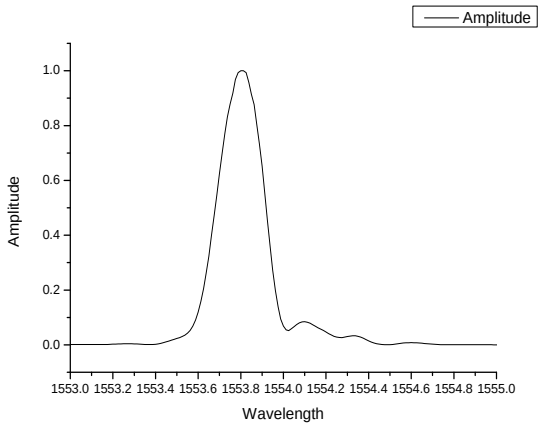

Figure 34- Spectrum of the FBG with Titanium buffer and Indium recoating at room temperature.

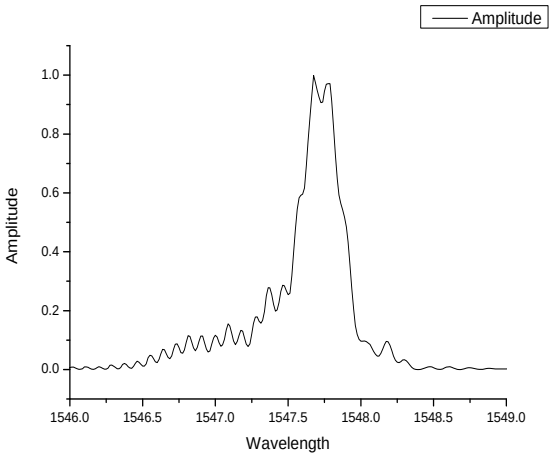

Figure 35- Spectrum of the FBG with Titanium buffer and Indium recoating at 78K.

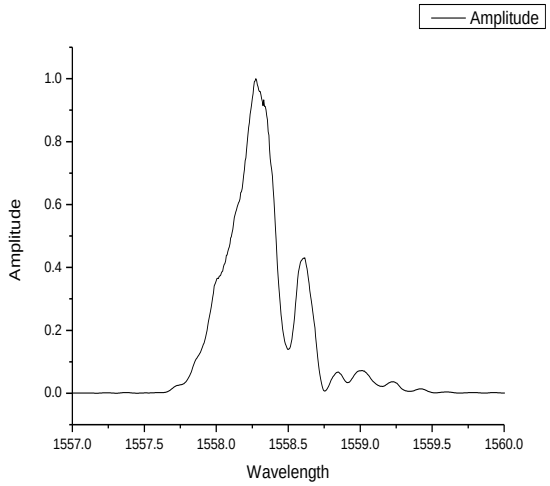

Figure 36- Spectrum of the FBG with Titanium buffer and Tin recoating at room temperature.

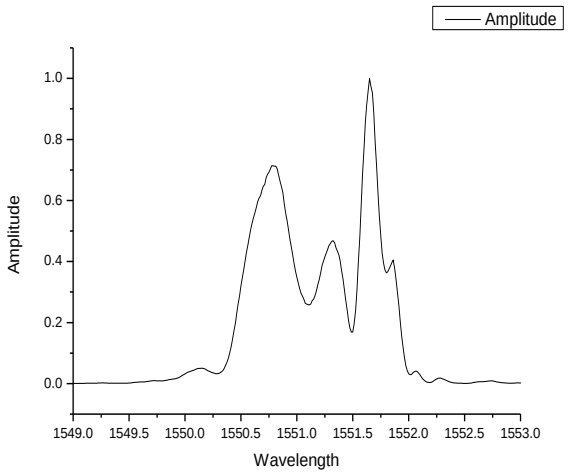

Figure 37- Spectrum of the FBG with Titanium buffer and Tin recoating at 78K.

By analysis of Figures 34 to 37 it can be seen that there are no significant alteration on the aspect of the Indium sensor spectrum at room temperature and at 78K, while in the case of the Tin sensor there is a new maxima suppressing the original one. This is due to the construction method used being unable to ensure the grating was centered and that there was no residual tensions on the grating due to different cooling rates of the metal.

Despite this behavior it was possible to measure a wavelength shift of 7.71 nm in the case of the Indium sensor and 8.8 nm in the case of the Tin sensor. This value for Tin is assuming the original maximum not the one who appeared with cooling.

According to "NBS29" a book of standards with data on the Coefficients of Thermal Expansion and their behavior with temperature the Indium sensor should have higher sensitivity than the Tin one. The fact that the Tin sensor had more sensitivity proves that he had better adhesion to the Titanium buffer and that a new buffer should be used for Indium.

Second Test

This new test was done using 200nm Cr buffers and was in every other way conducted similarly to the previous.

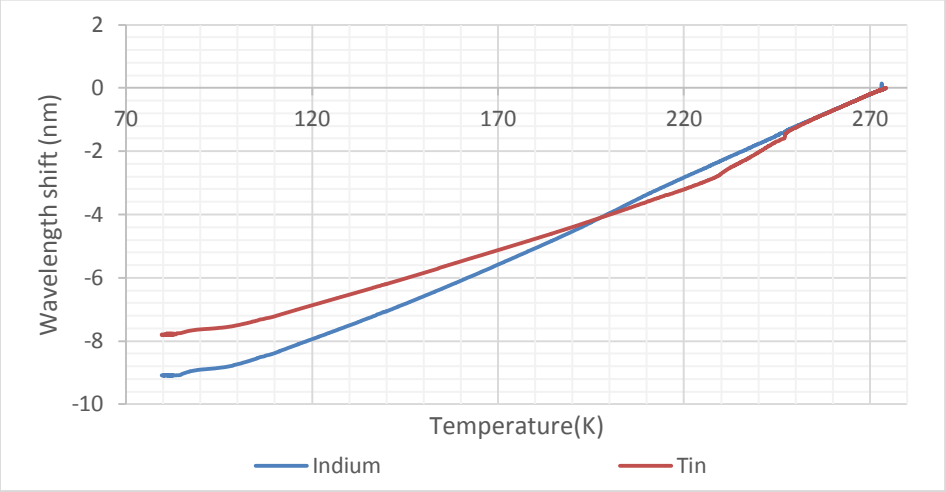

Figure 38- Wavelength shift with temperature of FBGs with 200 nm Chromium buffers one with recoating of Indium and the other a Tin alloy.

In Figure 38 we can observe the wavelength shift with temperature for this new buffer. With this buffer we can see a significant increase in the sensitivity of the Indium sensor with an almost linear behavior for all the temperature range. A greater sensitivity was also obtained for lower temperatures with both sensors, and by the curves appearance it is expected that the sensitivity is still significant at even lower temperatures.

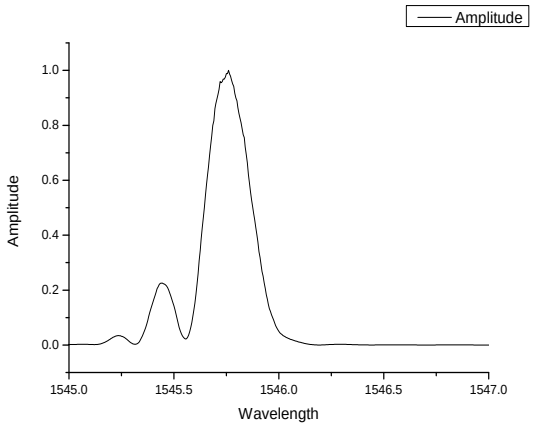

Figure 39- Spectrum of the FBG with Chromium buffer and Indium recoating at room temperature.

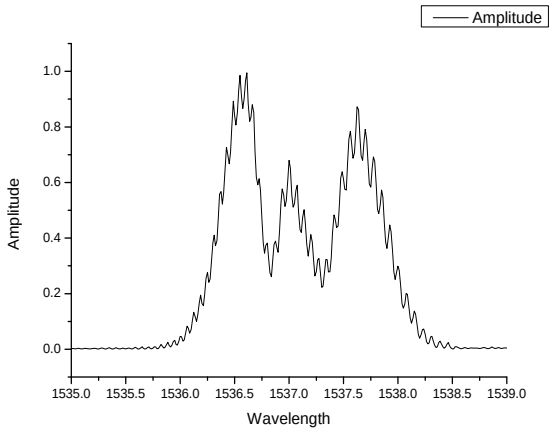

Figure 40- Spectrum of the FBG with Chromium buffer and Indium recoating at 78.

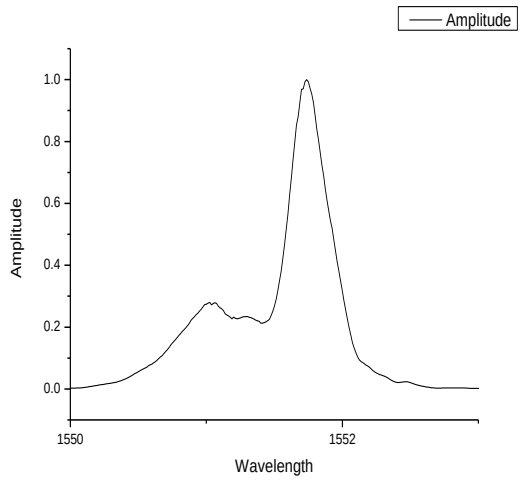

Figure 41- Spectrum of the FBG with Chromium buffer and Tin recoating at room temperature.

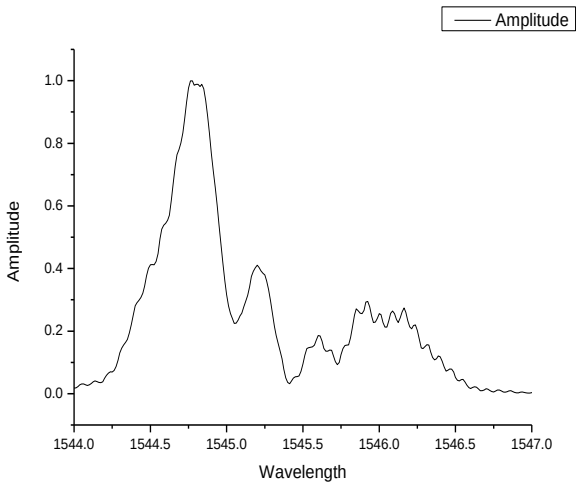

Figure 42- Spectrum of the FBG with Chromium buffer and Tin recoating at 78K.

The spectra can be seen in Figures 39 to 42 for both sensors at room temperature and at 78K.

Although the spectrum for the Tin sensor at 78K presents a clear maximum the same does not occur in the case of the Indium sensor where there are three different maxima. Despite this fact and due to the data acquisition software it was possible to track the real maximum. The software recorded all values and only one maximum was present during all the heating process, the one used to build the graph in Figure 38.

In this second test it was measured a wavelength sift of 9.3 nm in the case of the Indium sensor and 8 nm in the case of the Tin one.

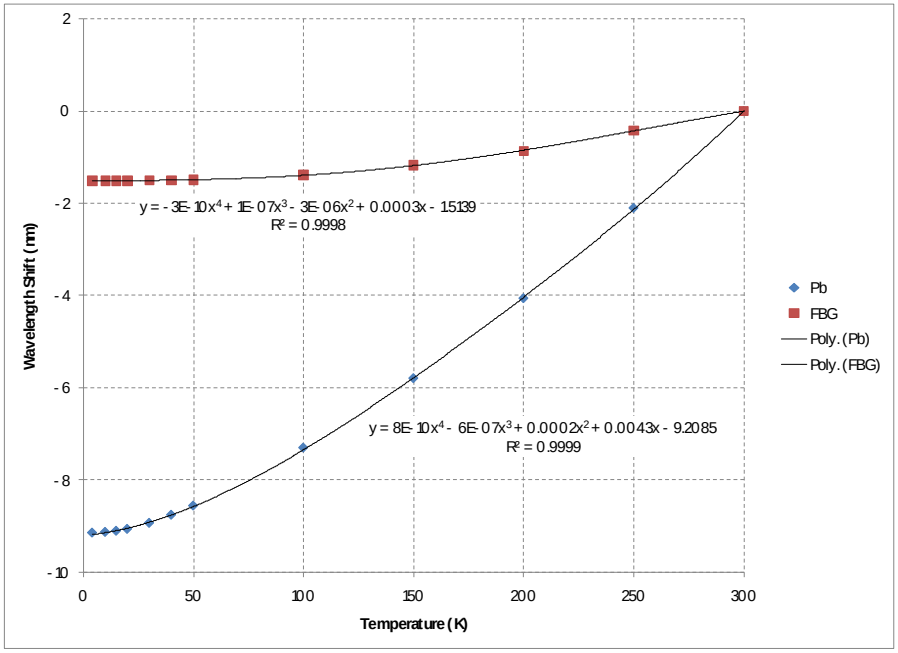

Figure 43- Wavelength shift with temperature of FBGs one with no recoating and the other glued to a Lead substrate.

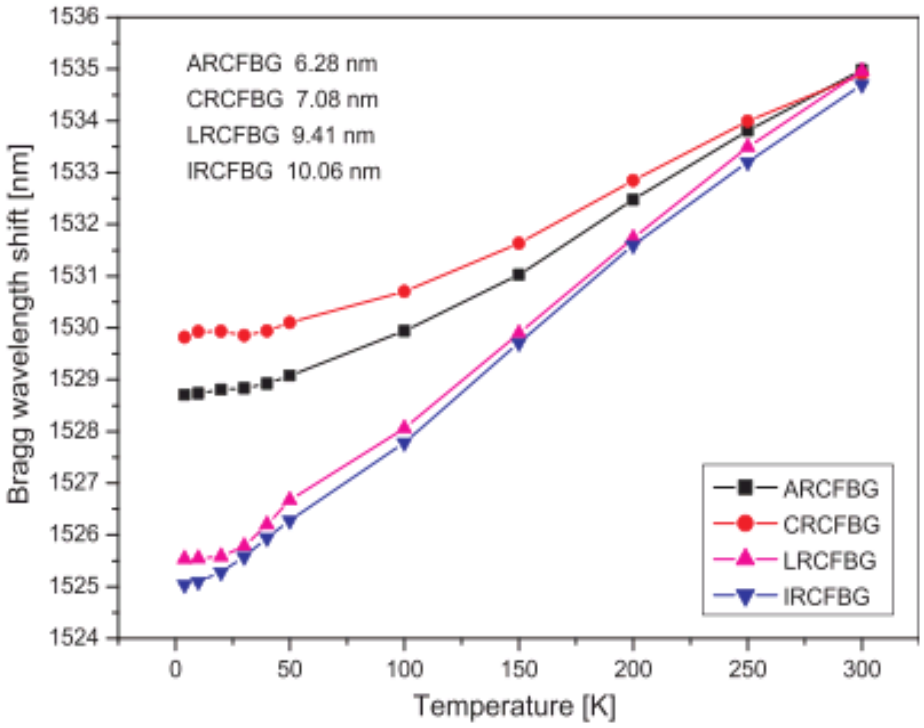

Figure 44- Wavelength shift with temperature of FBGs with different recoating metals.

This data was compared with the one previously obtained in the Lead sensor by FiberSensing (Figure 43) and the one on Dr. Ramalingam article "Performance evaluation of metal-coated FBG sensors for sensing low temperature" (Figure 44).

If the data obtained in this tests was reproducible using better equipment, the sensor constituted by a FBG with a 200nm Chromium buffer and Indium recoating would present higher temperature sensitivity than the ones represented in Figures 43 and 44 for the same temperature range. The same could be said for the FBG with 200nm Titanium buffer and Tin recoating if not for the fact that it has no sensitivity below 93K.

These were promising results and the spectra quality could be much improved with better casting setups. Although the sensor showed sensitivity to temperatures above 77K this is not the goal temperature range for this project so a test was initiated in order to determine the maximum wavelength shift between room temperature and 4.2K, temperature of liquid Helium.

SQUID test

In this test the Superconducting Quantum Interference Device was used not because of its own measuring capabilities but only because it was at the time the only device available to reach 4.2K with controllable temperature. This device's usage was provided by IFIMUP-IN and the sensor being measured was the one with 200 nm Chromium thin film and Indium recoating.

Due to this device mechanical setup that maintained the vacuum inside the measuring chamber a special feedthrough had to be used in order to read the wavelength shift from the FBG sensor. This feedthrough was provided by FiberSensing that already had done similar tests.

The measurements were made using the FS2200-BraggMETER from FiberSensing and a LabVIEW software written for this purpose that read the wavelength shift from the sensor and the temperature from the SQUID's computer logbook.

The temperature in the vacuum chamber where the FBG sensor was placed was controlled by the SQUID's computer, using its own software. First the temperature was made to drop to 4.2 K were it remained for 30 min, warmed to 10 K, then it was warmed up in steps of 10K at a time, where the temperature was maintained for 15 min until reaching 80K. After this temperature the amplitude of the steps were changed to 25K waiting for 15 min on each step.

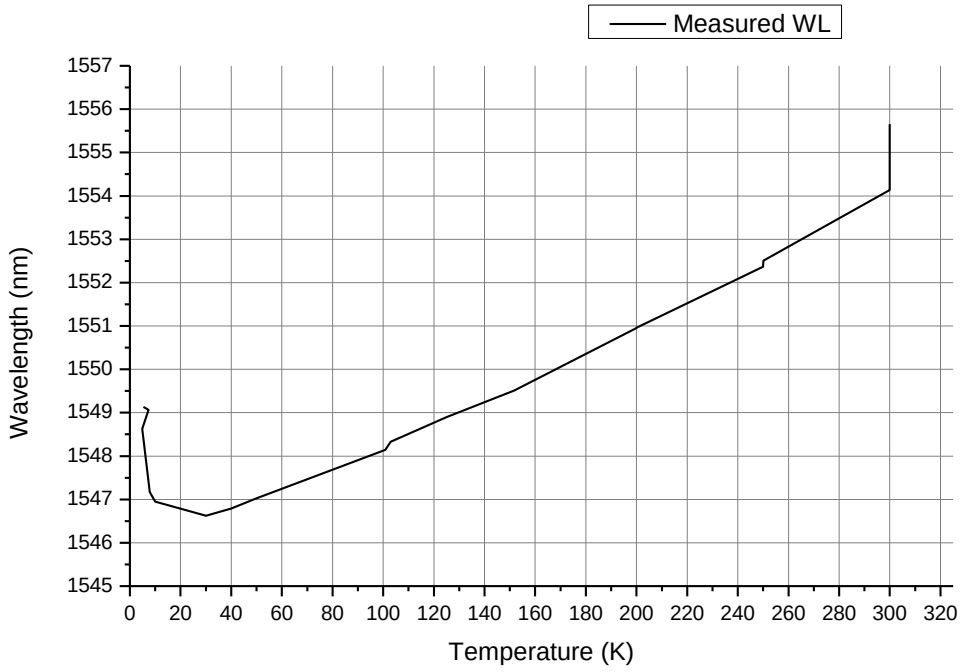

Figure 45 Wavelength measured during warm up from 4.2 to 300K during a SQUID test.

After data analysis it was clear that the temperature measured by the SQUID's computer did not match the real temperature sensed by the FBG sensor and that the temperature steps were not visible.

Figure 45 shows the collected data, matching the SQUID's temperature with the wavelength measured by the BraggMETER. At 4.2K when the warm up started the wavelength value should be at its lowest value instead as the temperature increased to 30K that value was still dropping. When the SQUID's temperature reached 300K and the FBG sensor was removed from the chamber there is an instantaneous increase of the wavelength value.

Data in this test was considered invalid, because it was impossible to determine the effective temperature in the FBG sensor at the time of the measurement. Although the linear behavior seen in the graph of Figure 45 until "30K" suggests sensitivity of the sensor below this temperature. The fact that the total wavelength shift is consistent with the one depicted in Figures 43 and 44 taking in account 4.2 K were never reached supported the decision of further develop this assembly technique.

Sensor construction and calibration tests

Construction

Once the construction technique was established as well as the thin film pre-coatings were specified, a series of tests were prepared. These tests intended to determine the temperature sensitivity of Indium and Lead recoated FBG sensors as well as the effect of the thin film buffers thickness.

To implement these tests a series of 36 gratings were pre-coated with the following films:

Table 2 Thin film Buffers used for sensor construction

Quantity	Thin Film Composition
6x	100 nm Ti
6x	200 nm Ti
6x	100 nm Cr
6x	200 nm Cr
6x	50 nm Cr + 50 nm Ni
6x	150 nm Cr + 18.5 nm Ni

The films with Cr + Ni were inserted in this study because according with [36] Ni has a good adhesion to In and Ni has a good adhesion to Cr.

With the help and support of FiberSensing a small oven with electronically controlled resistance was designed for sensor manufacturing. Molds were 15 mm long and 2.5 mm diameter, they were made in steel to produce Lead coated FBG sensors and peek to produce the Indium recoated ones. The mold's materials were chosen so that the casting metals had no adhesion to the mold, being easy to disassemble. The casting setup also contained two magnetic clamps to hold the grating in place during casting, a thermocouple and a Eurotherm 2139 temperature controller loaned by IFIMUP-IN.

At this point in order to have access to a temperature sensor calibration facility equipped with everything needed for multi sensor testing and calibration the author joined the Karlsruhe Institute of Technology (KIT) for a three months internship. At KIT the author was aggregated to the Cryogenics group of Institute of Techniqueal Physics (ITeP) under Dr. R.K. Ramalimgam supervision.

During the first month a plan for the sensors test and calibration was drawn. It was possible to get familiarized with the equipment to be use and protocol for its usage,

rebuilt the casting setup and wrote a LabVIEW program to enable all measurements to be automatized.

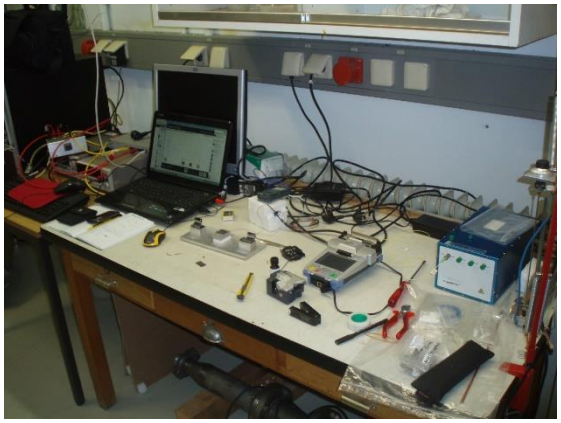

Figure 46 Entire casting setup used for FBG coating and spectrum monitorization.

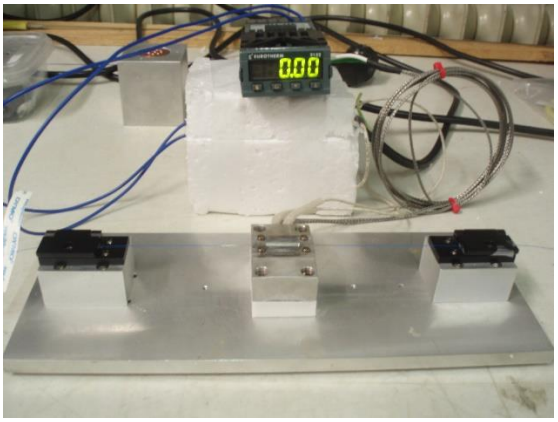

Figure 47 Casting setup with temperature control used for FBG coating

The LabVIEW software was written in a way that allowed for communication with a FiberSensing's BraggMETER for wavelength measurement and spectral analysis, and with a Keithley 2701 digital multimeter (DMM) that would read the values from a PT-1000 temperature sensor. The data collected from the DMM and BraggMETER would be saved in text files with a date and time stamp, and a folder would be created to store the spectra from each channel of the BraggMETER every time a measurement was made. The entire setup used is shown in Figure 46, in particular the casting setup can be seen in Figure 47.

After the software was ready and necessary equipment was made available the casting setup was built, and the sensor construction started, being the spectrum of each sensor always monitored for deformation. The Eurotherm controller was not compatible with the thermocouple provided with the casting setup. This led to an impossibility of accurate temperature measurement and control. The Eurotherm controller was used then to determine the amount of electric power that would be provided to the resistance, being this amount of power and its supply time optimized so that it would be just enough to melt the metals.

The sensors previously coated with the films described in Table 3 were then divided in the following twelve series.

Table 3 Diferent series of sensors to be constructed

Series	Thin Film Coating	External

		Coating
S1	100 nm Ti	In
S2	100 nm Ti	Pb
S3	200 nm Ti	In
S4	200 nm Ti	Pb
S5	100 nm Cr	In
S6	100 nm Cr	Pb
S7	200 nm Cr	In
S8	200 nm Cr	Pb
S9	50 nm Cr + 50 nm Ni	In
S10	50 nm Cr + 50 nm Ni	Pb
S11	150 nm Cr + 18.5 nm Ni	In
S12	150 nm Cr + 18.5 nm Ni	Pb

Every sensor was catalogued and marked after construction so it could be recognizable at any time, and no doubts about its coatings could appear in the future.

During the casting process polyamide 400 µm tubes 10 mm long were place on what would be the edges of the sensors in a position where they would not cover the grating but would intermediate between the coated and uncoated parts of the fiber reducing the chances of breaking. Even with extreme care there were some sensors that broke in that region on one of the sides still being usable for tests but 3 of them broke on both sides becoming unusable.

The sensors with more tendency to break were the ones with Pb coating due to the fact that were subjected to higher temperatures and no annealing. The temperature shock that the sensors were subjected when placed and removed from the small oven could have been responsible for the breaking.

First calibration

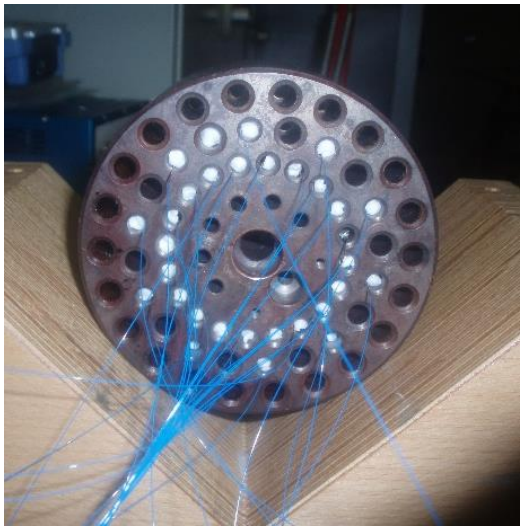

Figure 48 Copper block used for cryogenic temperature tests containing all FBG sensors constructed

Figure 49 Cryostat used for the first tests with all FBG sensors.

Taking the sensors that were usable, 4 arrays of 8 sensors spliced together were created, being arranged so that each sensor in an array had a different resonant wavelength. These sensor arrays were then placed inside cylindrical holes that went through a test block made of Copper and hold in place by Styrofoam balls. On this block a PT-1000 temperature reference sensor was also inserted in the center. The entire setup was then inserted inside a cryostat with feedtroughs for optical and electrical communication with respectively the BraggMETER and the DMM. The calibration block and the cryostat can be seen in Figures 48 and 49.

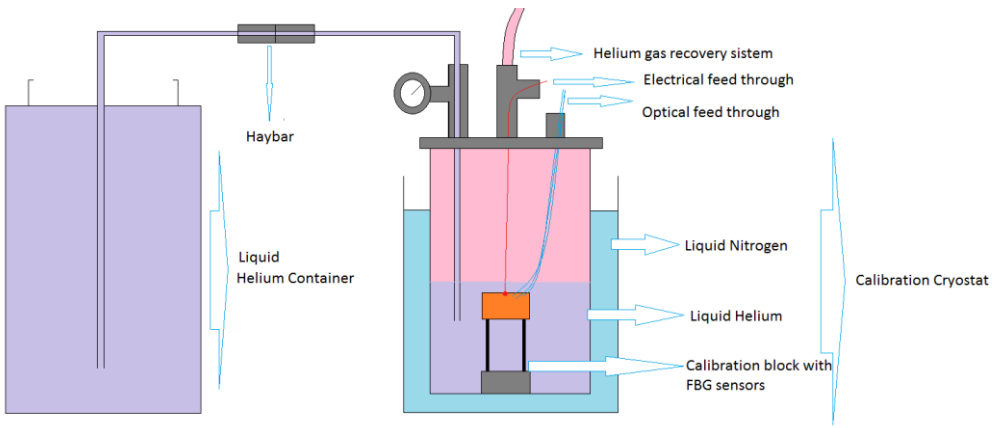

Figure 50 Calibration setup for the first tests.

The cryostat was then closed and connected to a He recovering system existent in the laboratory for He recycling, and pressure gauges that would allow for pressure monitoring inside the cryostat. When a vacuum pump was connected to the cryostat it was noticed that there was a leak on the optical feedtrough, once there was no need for this vacuum except to help with the He transference this was ignored. In order to ensure different pressure between the He container and cryostat pressure was increased inside the container using He gas.

The cryostat was then put on a Nitrogen bath to avoid fast temperature change inside the He chamber and a fast warm-up. Liquid He was then poured in from its container using a 'haybar' until the test block inside was covered at this point the He flow was stopped and the entire setup was left to warm up to 80K. Figure 50 represents the experimental setup and all equipment used with exception for the measuring units.

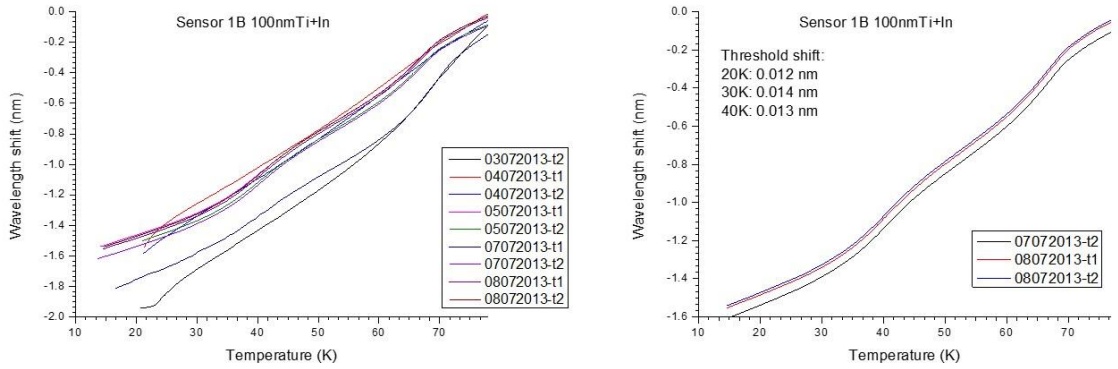

Figure 51 Sensor 1B 100nmTi+In wavelength shift during warm-ups for all nine cycles and then only for the last three showing repeatability

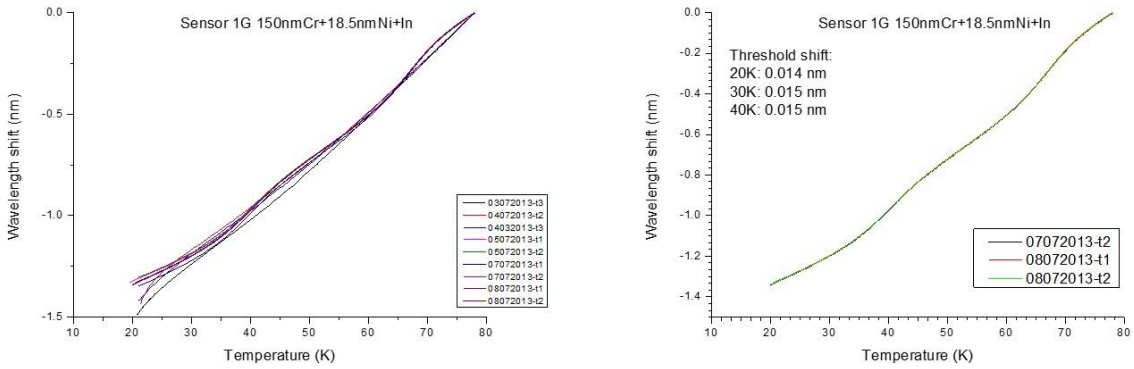

Figure 52 Sensor 1G 150nmCr+18.5nmNi+In wavelength shift during warm-ups for all nine cycles and then only for the last three showing repeatability

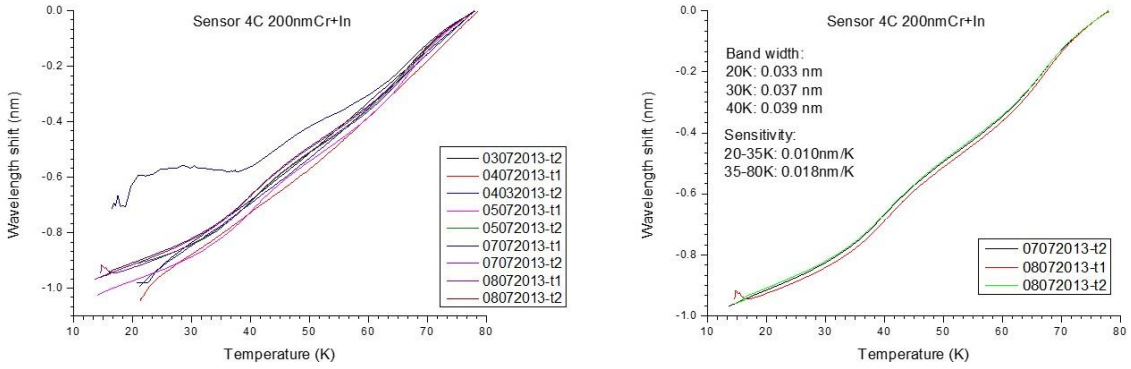

Figure 53 Sensor 4C 200nmCr+In wavelength shift during warm-ups for all nine cycles and then only for the last three showing repeatability

A total of nine temperature cycles were done between 4.2 and 80K to anneal the FBG sensors behavior in this thermal region and to remove internal stresses existent in the coating materials. There were some changes in the wavelength shift of the sensors in the first six cycles, but in the last three cycles the behavior was very similar in every sensor, sometimes appearing just some offset but not a chance in the slope. This process of making a sensor go through several temperature cycles is called temperature training and for the nine cycles done in this project a period of 10 days was needed.

Figures 51 to 53 show the wavelength shifts of three sensors with different buffers for all warm-ups and focus on the last three, showing that this annealing is necessary and independent from the buffer coating. When adding the analysis of Figures 53 to 72, it's also possible to affirm that the same happens for the sensors with Lead coatings. The same analyses was not made for the cool-down process once this was too fast due to the fact that liquid He was being poured inside the cryostat at a high flow rate, although this flow wasn't able to be measured.

The graphs of the last three warm-ups of each sensors were used to determine these sensors temperature sensitivity giving special attention to the temperature range between 20 and 40K.

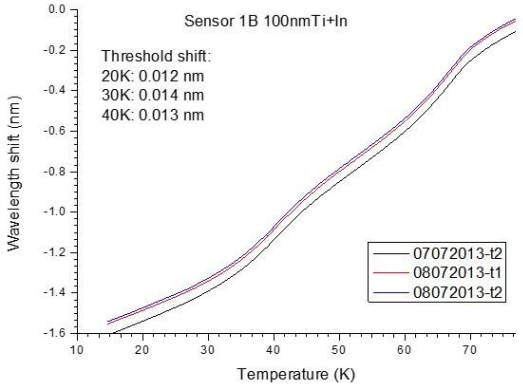

Figure 54 Sensor 1B behavior of wavelength shift with temperature for the last 3 cycles measured showing repeatability and small threshold shift between 20 and 40K

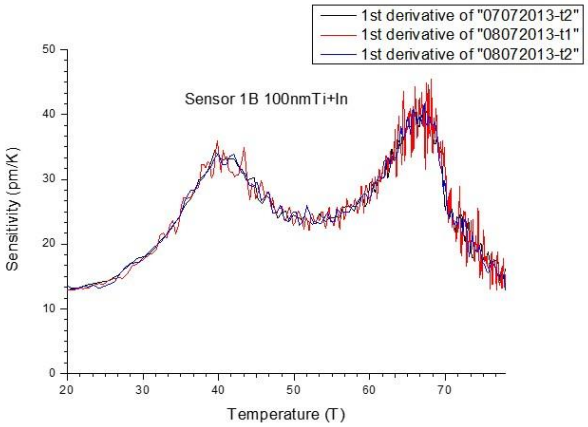

Figure 55 Sensor 1B sensitivity variation with temperature for the last 3 cycles measured showing regular sensitivity in all cycles

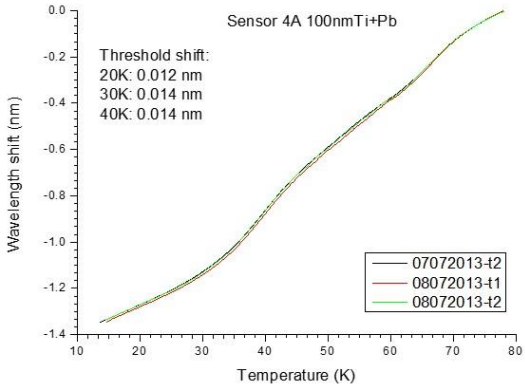

Figure 56 Sensor 4A behavior of wavelength shift with temperature for the last 3 cycles measured showing repeatability and small threshold shift between 20 and 40K

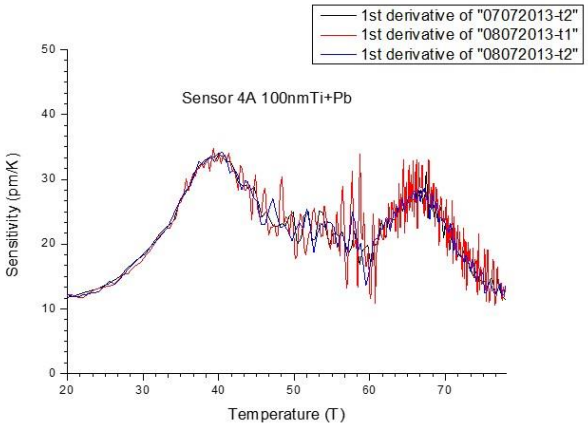

Figure 57 Sensor 1B sensitivity variation with temperature for the last 3 cycles measured showing regular sensitivity in all cycles

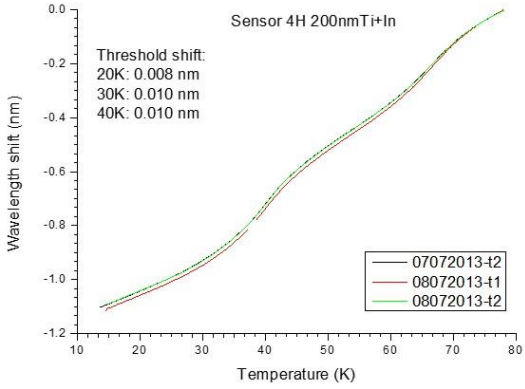

Figure 58 Sensor 4H behavior of wavelength shift with temperature for the last 3 cycles measured showing repeatability and small threshold shift between 20 and 40K

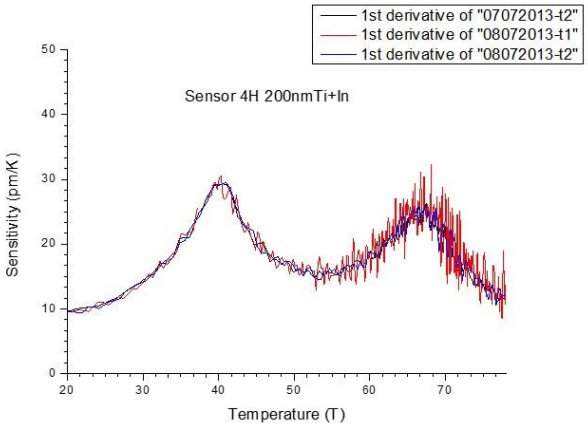

Figure 59 Sensor 1B sensitivity variation with temperature for the last 3 cycles measured showing regular sensitivity in all cycles

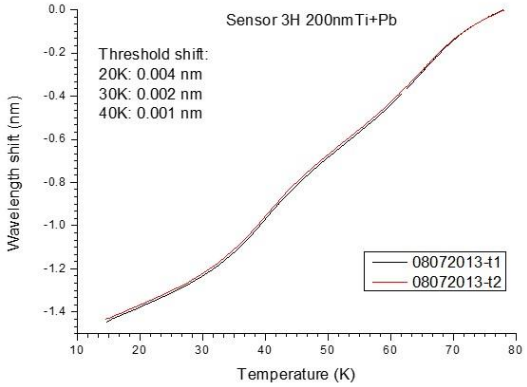

Figure 60 Sensor 3H behavior of wavelength shift with temperature for the last 3 cycles measured showing repeatability and small threshold shift between 20 and 40K

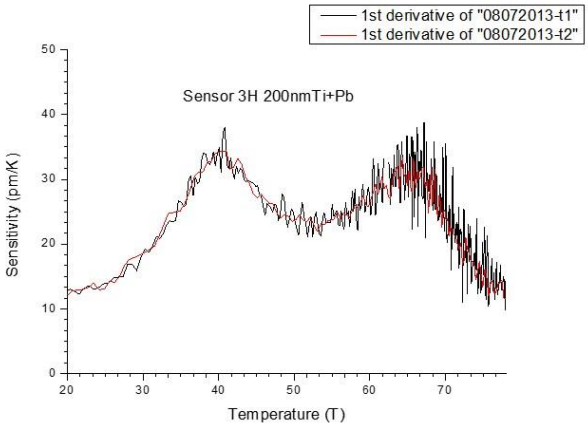

Figure 61 Sensor 1B sensitivity variation with temperature for the last 3 cycles measured showing regular sensitivity in all cycles

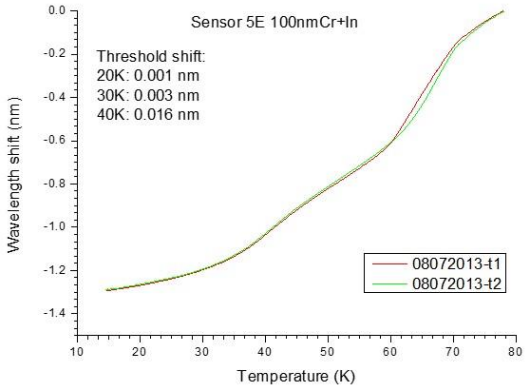

Figure 62 Sensor 5E behavior of wavelength shift with temperature for the last 3 cycles measured showing repeatability and small threshold shift between 20 and 40K

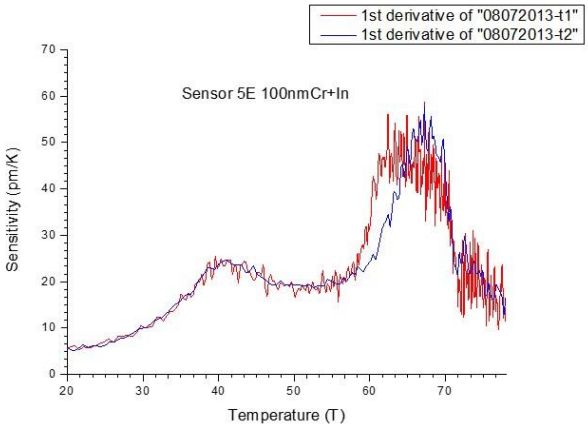

Figure 63 Sensor 1B sensitivity variation with temperature for the last 3 cycles measured showing regular sensitivity in all cycles

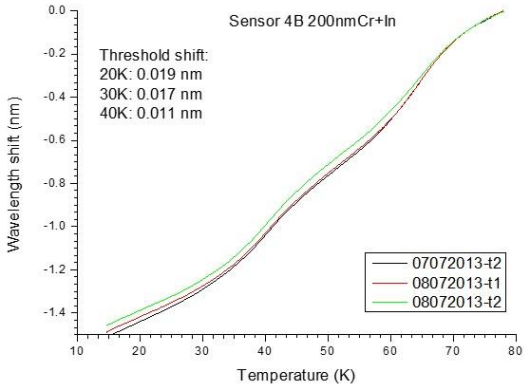

Figure 64 Sensor 4B behavior of wavelength shift with temperature for the last 3 cycles measured showing repeatability and small threshold shift between 20 and 40K

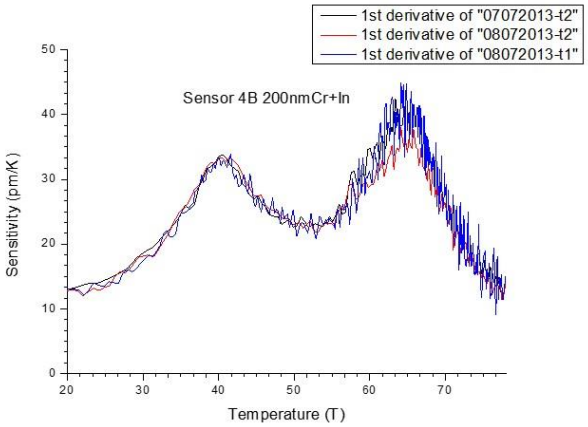

Figure 65 Sensor 1B sensitivity variation with temperature for the last 3 cycles measured showing regular sensitivity in all cycles

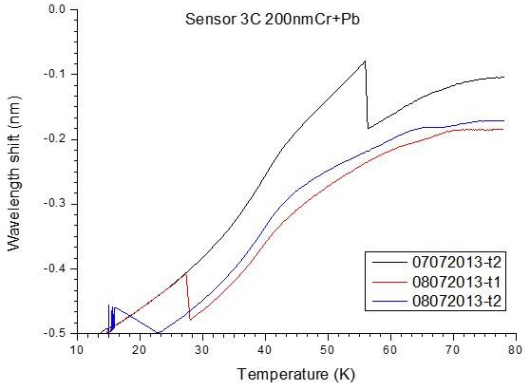

Figure 66 Sensor 3C behavior of wavelength shift with temperature for the last 3 cycles measured showing some repeatability but with high threshold shift

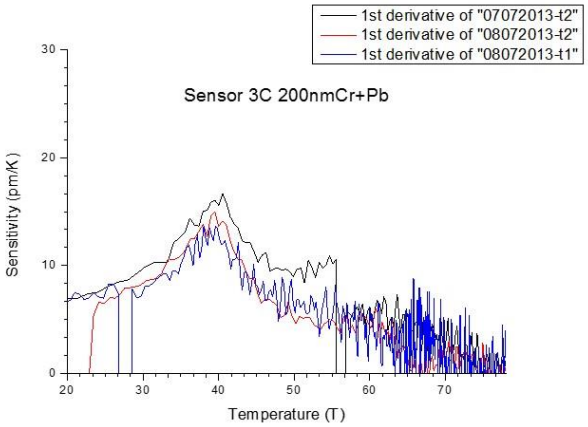

Figure 67 Sensor 3C sensitivity variation with temperature for the last 3 cycles measured showing regular sensitivity in all cycles

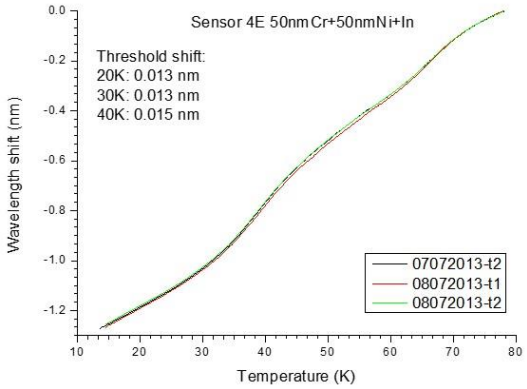

Figure 68 Sensor 4E behavior of wavelength shift with temperature for the last 3 cycles measured showing repeatability and small threshold shift between 20 and 40K

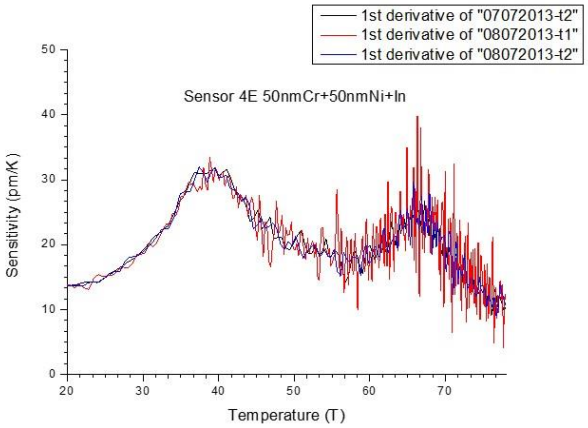

Figure 69 Sensor 1B sensitivity variation with temperature for the last 3 cycles measured showing regular sensitivity measured in all cycles

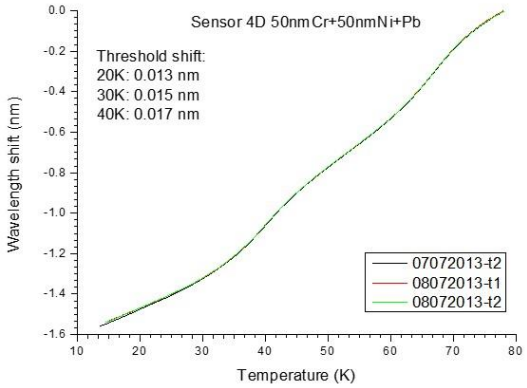

Figure 70 Sensor 4D behavior of wavelength shift with temperature for the last 3 cycles measured showing repeatability and small threshold shift between 20 and 40K

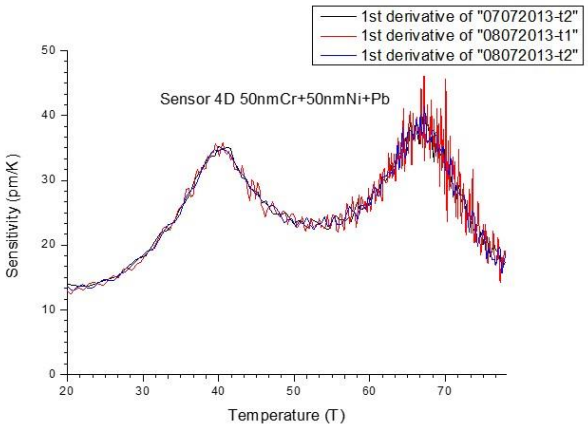

Figure 71 Sensor 1B sensitivity variation with temperature for the last 3 cycles measured showing regular sensitivity measured in all cycles

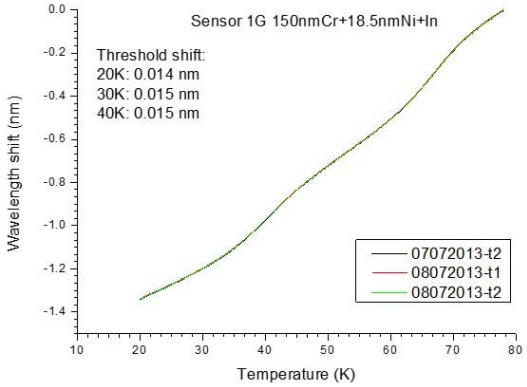

Figure 72 Sensor 1G behavior of wavelength shift with temperature for the last 3 cycles measured showing repeatability and small threshold shift between 20 and 40K

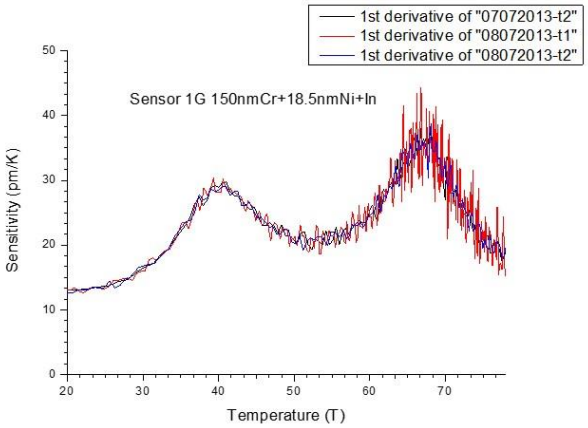

Figure 73 Sensor 1B sensitivity variation with temperature for the last 3 cycles measured showing regular sensitivity measured in all cycles

Figures 54 to73 show the wavelength shift and sensitivity curves for 10 of 12 series programed. All sensors for series S6 and S12 described in Table3 were unable to be measured because during the construction process three were broken and during the first cool down the thermal shock broke an already fragile splice in one of the arrays separating the last three sensors corresponding to these series.

Apart from sensor 3C all other sensors present a very regular repeatable behavior and sensitivity, the sensitivity curves all appear to present the same behavior. It would be expected to obtain a systematic growth in sensitivity with the temperature warm-up. This wave like behavior that also appears in the wavelength shift graphs in a more subtle manner that is a result of the reference sensor polynomial fit introduced on the measuring software. A sixth degree polynomial fit was calculated to translate the voltage read by the DMM in a temperature value saved by the software.

Table 4 Sensitivities at diferent temperatures for sensors of 10 diferent series

	Sensitivity pm/K											
	S1	S2	S3	S4	S5	S6	S7	S8	S9	S10	S11	S12
Temp.	1B	4A	4H	3H	5E	Broken	4B	3C	4E	4D	1G	Broken
20K	13	0.012	10	13	05		13	07	14	13	13	
30K	18	0.019	15	19	10		18	08	19	17	17	
40K	34	0.034	29	35	25		34	14	30	35	29	
50K	25	0.025	16	23	17		23	07	20	24	20	
60K	29	0.017	19	29	32		30	05	19	26	25	
70K	25	0.023	22	23	36		28	03	21	32	31	
Buffer	100nmTi		200nmTi		100nmCr		200nmCr		50nmCr+50nmNi		150nmCr+ 18.5nmNi	

Table4 resumes the sensitivities at different temperatures of different FBG sensor series for a more clear analysis. Series with odd numbers represent Indium coatings while the ones with even number represent coating with Lead, and every even numbered series has the same coating as the previous.

Taking in account this data there seems to be no significant changes in sensitivity between sensors with the same buffer material except in the case of Cr buffers were for the same coating 100nm film didn't seem to be enough. As sensor 5E and 3C were the only ones from series S5 and S8 respectively to survive the entire process of construction and measurement in this work no definitive conclusions will be taken with relation only to these sensors.

There is insufficient data in this study when it comes to Lead coated gratings so comparison with the ones coated with Indium could lead to false conclusions. In this sensors there seems to be no clear advantage in using Indium or Lead being the sensitivities obtained for the temperature range studied acceptable when taking in account the measuring devices needed for their use.

Figure 74 Test block used for the first tests when removed from the cryostat

When the sensors were removed it was noticed that some sensors have detached from the copper block, as can be seen in Figure 74. This could mean that some sensors

were not measuring the same temperature as the reference sensor. As the cryostat was a closed environment thermally protected by a Ni bath the difference in temperature felt by reference sensor and FBGs couldn't be high. Although this difference was not measured there are no visible difference in the *Wavelength shifts (T)* graphs between sensors that detached from the block and those that kept attached to it with exception to the residual wave like behavior previously discussed.

Final calibrations

From the first analysis 20 sensors were chosen to undergo more temperature cycles on a standard cryogenic temperature sensor calibration facility at the KIT facilities. Two new sensors were also inserted in this test without undergoing thermal annealing, these sensors consisted of two FBG glued with Stycast-2850 FT and catalyst 24LV to a block (2x2x20mm) of zirconium tungstate. This material was only made available at this point and due to its Negative Coefficient of Thermal Expansion it was decided to study its behavior at cryogenic temperature.

A setup has been constructed to accommodate these sensors, this setup was made in copper that underwent temperature treatment and had very precise measurements in order to fit in the calibration cryostat. The sensors were rolled around this block on veins carved for that purpose, during this process the sensors were being monitored so that there were no losses caused by tensions on the fibers due to bending or stretch. In order for the sensors not to detach from this block, it was covered with kapton tape.

Figure 75 Calibration block with all the FBG sensors as it was placed inside the Standard Calibration Cryostat

Figure 76 Calibration block connected to its support where all feedtroughs were connected before placement inside the Standard Calibration Cryostat

Figures 75 and 76 show the calibration block that hold the sensors and the entire measuring apparatus with the reference sensor that was inserted inside the cryostat.

Figures 75 and 76 show the calibration block that hold the sensors and the entire measuring apparatus with the reference sensor that was inserted inside the cryostat.

Once the sensors were placed inside the cryostat the control of the temperature was achieved by adjusting the He mass flow. Temperature was monitored by both the standard temperature calibration reference sensor and a PT-1000 calibrated sensor connected to the measuring system that was used in the first calibration. This PT-1000 sensor was calibrated but showed no sensitivity below 16K so we only used the data collected from this sensor for temperatures above 20K.

Contrary to the authors knowledge the temperature measured by the standard calibrated sensor was not being automatically measured and stored in any digital document for future comparison with the temperatures with the PT-1000 sensor. So these values had to be read and noted manually and every time the system had to receive a new command to change temperature or mass flow that had to be done manually.

A plan had been established to make three cycles between 300 and 10K followed by three cycles between 80 and 10K followed by temperature steps of one hour in the temperatures of 10, 20, 27, 29, 31 and 40K.

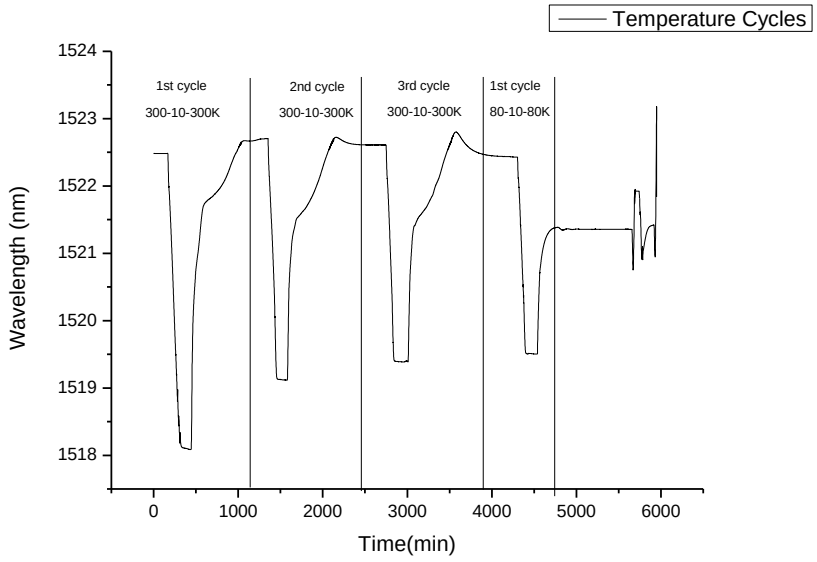

Figure 77 Wavelength variation during all temperature cycles and steps for Sensor 1A

Figure 77 shows the wavelength variation since the beginning of the calibration for sensor 1A but the behavior of all other sensors were in every way similar to this one.

It's possible to see that is a considerable reduction in the maximum wavelength shift between the first 300-10-300K cycle and the rest. This sensors had undergone temperature annealing between 80 and 10K but not above this temperatures this result seen in Figure 77 comes from the lack of temperature annealing above 80K and is possible to see that with an increasing number of cycles the maximum wavelength shift tends to a regular value.

After the first 80-10-80K cycle most of the sensors started to loose amplitude at temperature below 40K, being that some spectra even disappeared below this temperature being impossible to measure. This effect is attributed to high losses induced by tight curvature. That is why the data obtained from the 80-10-80K cycles as well as temperature steps will not be treated or commented in this report.

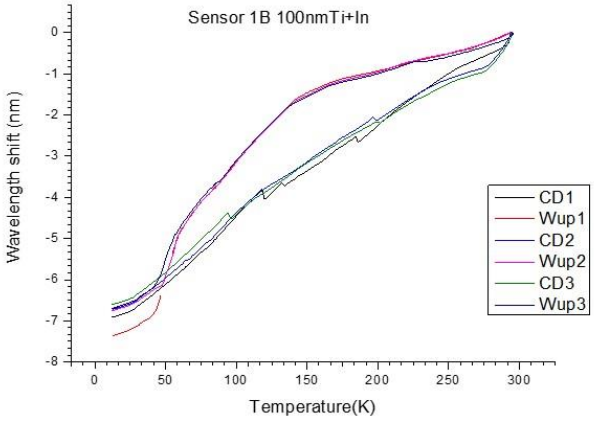

Figure 78 Cool-down and warm-up curves of the wavelength shift with temperature for sensor 1B during the three cycles between 300-10-300K

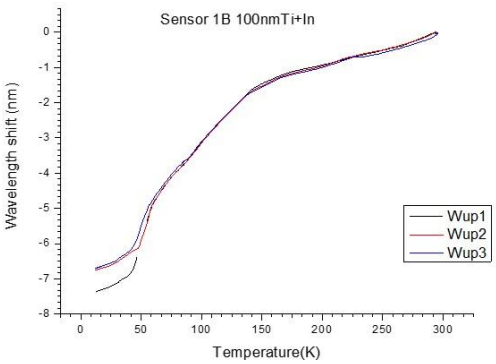

Figure 79 Warm-up curves of the wavelength shift with temperature for sensor 1B during the three cycles between 300-10-300K

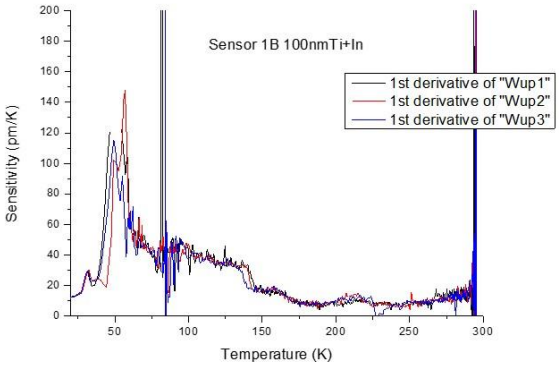

Figure 80 Sensitivity curves for sensor 1B during the three cycles between 300-10-300K

Figures 78 to 80 represent the behavior of Sensor 1B during the final calibration, this sensor represents the behavior of most sensors in this study, with exception for sensors 1G, ZT1 and ZT2 that will be discussed ahead.

For this sensor in the 300-10-300K cycles exists a very well defined hysteresis loop that wouldn't be a problem if the loop wasn't so large, since this sensor in particular shows great repeatability. It's the author's opinion that this behavior can come both from bending in the FBG sensor and a difference between the temperatures measured by the FBG and the PT-1000 reference sensor although the mass flow changes during the cycles could also have had some impact. This PT-1000 sensor was not centered with the calibration block once this position was occupied by the standard sensor and had to be fixed in one of the sides of the calibration block.

The warm-up curves were used to calculate the temperature sensitivity of these sensors between 20 and 300K as was previously done in the first calibration test, and although there is a minimum of sensitivity of 10pm/K this occurs both for temperatures of 20K and above 175K which is not expected. At higher temperatures the sensor is expected to have higher sensitivity, meaning that the sensitivity should always increase and never the opposite, this behavior comes from different warm-up rates seen in Figure 77 that increases the hysteresis and is responsible for the nonlinear behavior of the wavelength shift seen in Figure78.

This sensor like most of the other sensors cannot be used as a reference of behavior due to their large hysteresis loops and overall temperature behavior and sensitivity. The bending resulting from rolling the sensors in the block took a high impact in their behavior permanently altering their behavior. Although all precautions were taken and

all sensors monitored during their assembling in the calibration block the ductility of the coating materials was too high for the sensors disposition used.

The continuous temperature cycles could have also created contraction in the optical fibers rolled around the calibration block particularly in the splicing regions, these contraction could have created bending and/or crushing in the fibers creating high losses that prevented good measurements after the first 80-10-80K cycle.

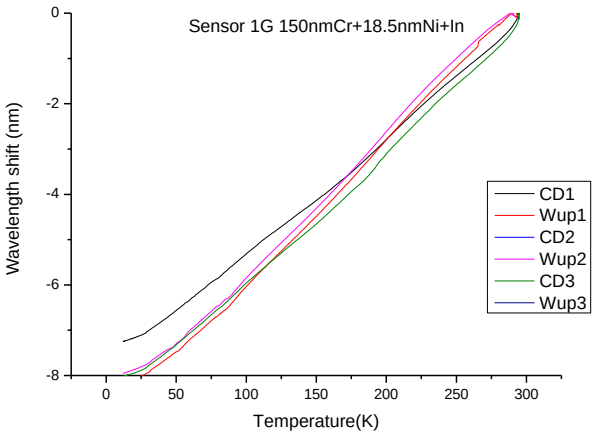

Figure 81 Cool-down and warm-up curves of the wavelength shift with temperature for sensor 1G during the three cycles between 300-10-300K

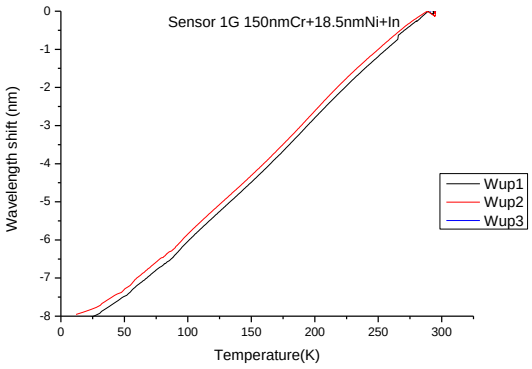

Figure 82 Warm-up curves of the wavelength shift with temperature for sensor 1G during the three cycles between 300-10-300K

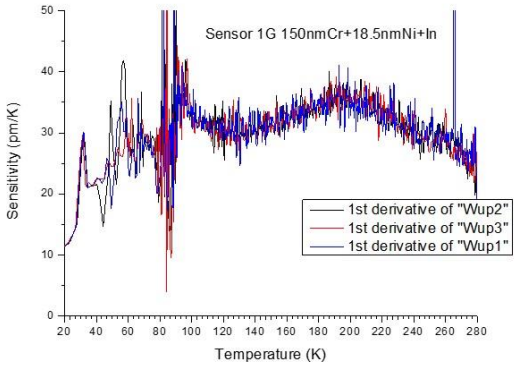

Figure 83 Sensitivity curves for sensor 1G during the three cycles between 300-10-300K

Sensor 1G was the only one to show the expected behavior from all other coated sensors built and its behavior is shown on Figures 81 to 83. It's possible to see some hysteresis close to 300K in Figure 81 were all 300-10-300K cycles are represented, but

in this case unlike other sensors the loop is very small and likely resultant from the different temperatures felt by FBG and the PT-1000 reference sensor.

When focusing only in the warm-up curves the linearity of the sensor's behavior is impressive translating in a high sensitivity of approximately 30pm/K for temperature above 80K with a minimum of 13pm/K at 20K which is very good for the temperature measurement equipment's resolution of 1pm/K.

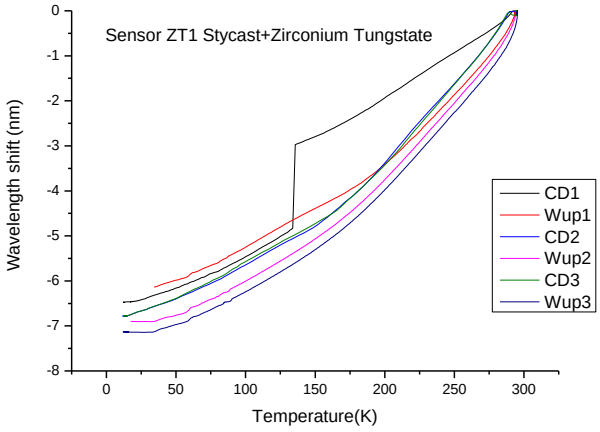

Figure 84 Cool-down and warm-up curves of the wavelength shift with temperature for sensor ZT1 during the three cycles between 300-10-300K

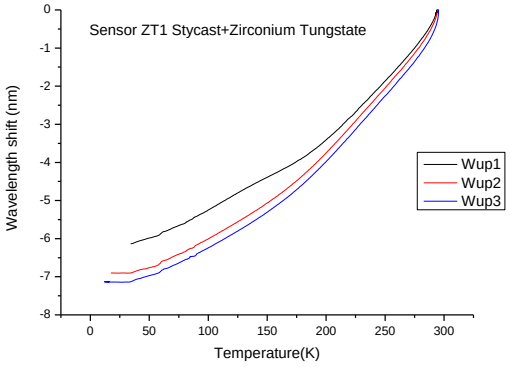

Figure 85 Warm-up curves of the wavelength shift with temperature for sensor ZT1 during the three cycles between 300-10-300K

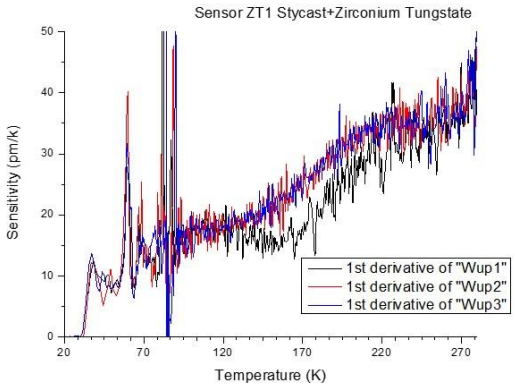

Figure 86 Sensitivity curves for sensor ZT1 during the three cycles between 300-10-300K

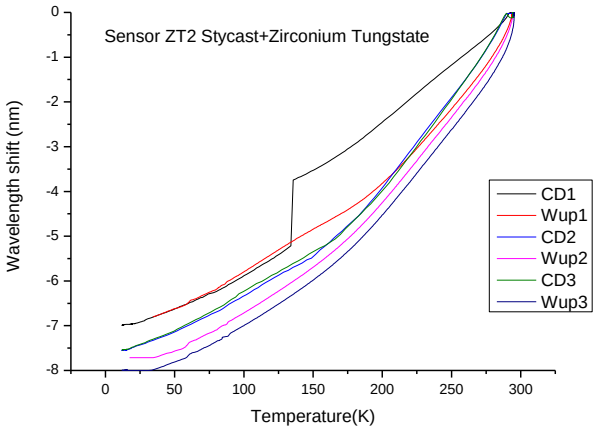

Figure 87 Cool-down and warm-up curves of the wavelength shift with temperature for sensor ZT2 during the three cycles between 300-10-300K

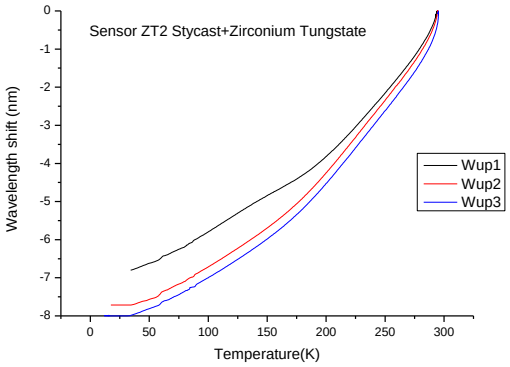

Figure 88 Warm-up curves of the wavelength shift with temperature for sensor ZT2 during the three cycles between 300-10-300K

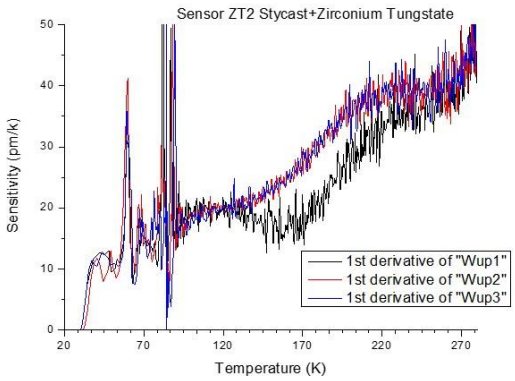

Figure 89 Sensitivity curves for sensor ZT2 during the three cycles between 300-10-300K

Sensors ZT1 and ZT2 had no bending what so ever, both due to the Zirconium Tungstate lack of ductility and the sensors position in the calibration block. Figures 84 to 86 correspond to the analysis of sensor ZT1 and Figures 87 to 89 to the analysis of sensor ZT2. Both sensors were attached to the same block of Zirconium Tungstate so they should present the same results.

For both sensors no hysteresis is observed in the 300-10-300K cycles and apart from the first cycle there seems to be repeatability of the warm-up curves rather than some slight offset.

In both sensors the sensitivity graphs show the same behavior with temperature, where a continuous increase in sensitivity with an increase in temperature. Once the substrate used in these sensors, the Zirconium Tungstate, has NCTE it was expected that these sensors had higher sensitivity at low temperatures than at higher ones. This material

volume reaches its maximum at 0K and minimum at 1100K like it is shown in Figure 10. It was also expected that this material presented the highest sensitivity at 0K instead the sensor only shows sensitivity above 35K.

This unexpected behavior for these sensors is most likely due to the sensor's construction technique, where the grating is fixed to the Zirconium Tungstate substrate with Stycast glue. Stycast's datasheet informs that the glue has low CTE, what could mean that it could be limiting the expansion of the grating with the material or even the material expansion itself. Explaining also why there is no sensitivity below 35K. The fact that sensor ZT1 has a maximum negative wavelength shift of 7nm and sensor ZT2 has a maximum negative wavelength shift of 8nm supports the theory that this construction technique was not the best for this kind of sensor and that the glue and catalyst used were having a major impact.

Conclusions

FBG coated sensors present a good solution for temperature monitoring in harsh environments where other sensors may not function properly due to the presence of high electromagnetic fields and radiation.

Coating techniques EBD and dip-coating are not recommended if both homogeneity and high thickness are necessary. Electrodeposition is the most promising technique for coating these sensors but to electrodeposit on metal coated fibers is not easy and takes a long period to optimize, for coating materials like the ones studied in this project with melting points below 400K casting has proven to be a more useful and cheaper technique with easier implementation.

Some coatings don't seem to have good adhesion to the fiber glass so the use of a buffer layer can be necessary, Chromium and Titanium have proven to have high adhesion to the fiber, an extra buffer layer could also be used to improve adhesion between the fiber and the coating material. Buffer layers don't need be more than 200nm to promote adhesion but need to be very homogeneous and cover all the grating surface, they are responsible for transmitting the coating expansion to the fiber and so should have high Young's modulus. No conclusion was reached related to the impact of the buffer layers on the FBG sensors sensitivity.

The coatings need to be at least 5 times thicker than the fibers diameter which is 125µm, once this means a considerable amount of material the sensor has to undergo temperature annealing to ensure it gives always the same response in future measurements. Although different gratings have different resonant wavelengths the wavelength shift with temperature should be the unit of measurement for these sensors.

The goal to create a coated FBG sensor capable of sensing temperatures between 20 and 40K was reached and sensitivities of 14pm/K at 20K were demonstrated, which is very good for temperature measurements using standard FBG interrogation equipment.

Future work

This work represents the first steps in the research and development of new FBG temperature sensors for cryogenic use. The results obtained provide only a glance of the future capabilities of these sensors and their construction techniques. Many things haven't gone according to plan as was expected, providing the author with important information on how proceed in future tests.

In future similar experiments the author proposes the FBGs used for sensor construction and testing should have resonant wavelengths at least 10nm apart to ease sensor's multiplexing in the same array. This fact alone would greatly facilitate the data analyses, ensuring that a bad sensor's spectrum do not overlap with the one from another sensor. Also creating arrays of gratings in the same fiber without splicing would greatly reduce the losses and the bending problems that led to signal loss in the final calibrations. Whenever possible sensors used for testing should be single units measured individually in their final packed form to avoid signal losses and deformation of the sensing element, while allowing the material to expand without constraints.

As the casting technique proved to be very effective in the sensor coating it should be perused ways to improve the coating homogeneity and reduce the fiber brittleness. For this purpose fibers with small grating windows of 10 to 15mm with polyimide coatings should be used. Polyimide coatings can go up to 400K without deterioration, which could help reduce breakage in the edges of the sensor. Also a more precise control of the casting temperature needed to melt the coatings followed by a slow cooling rate could help not also reduce breakage but reduce thermal stress in the material.

Different molds should be used for every coating, made in materials with higher melting temperature to hum the coating material have no adhesion. These molds should surround the entire grating not only at the base and should have a mechanism to remove the excess of material. Also to increase production and save in power consumption arrays of molds could be placed in the same oven when casting the same coating. The molds dimensions should be reduced as much as possible for faster temperature responses.

When conducting temperature training cycles these should be between the temperature range of all following tests and future usage. In these training cycles cooling and warming rates should be controlled and optimized for each cycle protecting the sensor from thermal shocks, avoiding the creation of thermal stress in the sensing element. This study should lead to a great reduction on the training time of these sensors.

The calibration blocks constructed should always ensure that the sensors can't get detached from them and the sensors aren't bent. Reference sensors should be always be placed in the center of the calibration block and when it's not possible more than one reference sensors to be used.

Data acquisition software should be used in order to obtain a more accurate set of data without offsets that could lead to wrong conclusions.

When using the SQUID magnetometer for temperature measurement and FBG sensor calibration a reference sensor should be inside the sample holder for temperature monitoring. If this is not possible the temperature should only be measured in steps and the time the sensor stays in each step should be optimized so it is long enough for the sensor to actually be at that temperature.

Future tests should also include a temperature response of the FBG sensors constructed with this technique, these tests were not conducted in this project because of permanent damage done to the sensors during the last calibration test.

Mercury is a material with high CTE higher than the other metals studied on this work, the use of this material should be further pursued for cryogenic temperature sensors through different techniques like capillary insertion on photonic-crystal fibers (PCF) with compositions that ensure the adhesion to this metal.

New coating materials should be studied and tested, not only metals but also alloys ceramics and specially polymers, they present the highest CTE of all materials referred in this work and could lead to good sensitivities at temperatures below 20K.

Sensors using Zirconium Tungstate or other subtracts should be constructed in a different way without adhesives over the grating section. Zirconium Tungstate and other materials with NCTE present a very good solution for temperature measurements below 20K. Coating FBGs with a polymer saturated with nanoparticles of one of these materials could be a solution for improving the sensitivity in this temperature range. This theory should be pursued and studies should be led to the find a good polymer and the optimal size of the nanoparticles.

There is a goal that future work in this subject should lead to a standardization of the calibration process for this sensors, leading to universal calibration polynomials for sensors built using the same exact materials and techniques. This would mean a sensor could be built and trained without constant motorization of spectrum and

wavelength shift variation and its behavior would still be described by the same calibration polynomial.

Bibliography

1. Temperature Sensors, https://controls.engin.umich.edu/wiki/index.php/Temperature Sensors. (accessed May 14, 2013).
2. Dr. Rajender Thusu, Frost & Sullivan. "Temperature Sensor Technology Transition and End-user Growth Trends." Sensors Mag, 16 December 2011.
3. Culshaw, B.; Dakin, J.P. Optical fiber sensors: applications, analysis and future trends - vol. 4. Artech House Publishers: Boston, London, 1997.
4. Krohn, D.A. Fiber Optic Sensors: Fundamentals and Applications - 3rd edition. ISA: New York, 2000.
5. Hill, K.O.; Fujii, Y.; Johnson, D.C.; Kawasaki, B.S. "Photosensitivity in optical fiber waveguides: Application to reflection filter fabrication." Appl. Phys. Lett., 1978, 32(10), 647-649.
6. Hill, K.O.; Meltz, G. "Fiber Bragg Grating Technology Fundamentals and Overview." Journal of Lightwave Technology, 1997, 15(8), 1263-1276.
7. Kashyap, R. Fiber Bragg Gratings. Academic Press: San Diego, 1999.
8. Othonos, A.; Kalli K. Fiber Bragg gratings: Fundamentals and Applications in Telecommunications and sensing. Artech House Publishers: Boston, London, 1999.
9. Othonos, A. "Fiber Bragg gratings." Rev.Sci. Instrum., 1997, 68(12), 4309-4341.
10. Erdogan, T. "Fiber Grating spectra." Journal of Lightwave Technology, 1997, 15(8), 1277-1294.
11. Reddy, P.S.; Srimannarayana, K.; Sai Prasad, R.L.N.S.; Sen Gupta, D.; Sai Shankar, M.; Kishore, P. "Enhancing the temperature sensitivity of fiber Bragg grating sensor using bimetallic strip." Proc. SPIE, 2012, 8351.
12. Walstrom, P. L. "Strain gauges for superconducting magnet testing." Cryogenics, 1980, 20(9), 509-512.
13. Habisreuther, T.; Ecke, W.; Latka, I.; Schröder, K.; Willsch, R. "Fiber Optic Bragg Grating Sensors at Cryogenic Temperatures." Proc. SPIE, 2010, 7653.
14. Kim, D.G.; Yoo, W.; Swinehart, P.; Jiang, B.; Haber, T.; Mendez, A. "Development of an FBG-based low temperature measurement system for cargo containment of LNG tankers." SPIE Optics East, 2007, 6770(12), 1-12.

15. Gupta, S.; Mizunami, T.; Yamao, T.; Shimomura, T. "Fiber Bragg grating cryogenic temperature sensors." Applied Optics, 1996, 35(25), 5202-5205.
16. Li, K.; Zhou, Z.; Liu, A. "A high sensitive fiber Bragg grating cryogenic temperature sensor." Chinese Optics Letters, 2009, 7(2), 121-123.
17. Rajini-Kumar, R.; Suesser, M.; Narayankhedkar, K.G.; Krieg, G.; Atrey, M.D. "Performance evaluation of metal-coated fiber Bragg grating sensors for sensing cryogenic temperature." Cryogenics, 2008, 48(3-4), 142-147.
18. Wang, Q.; Fen, Z.; Deng, F.; Huang, G.; Yan, L.; Dai, Y. "Fiber Bragg gratings for strain sensing in high temperature superconducting magnet." IEEE Transactions on Applied Superconductivity, 2007, 17(2), 2377-2380 .
19. Lupi, C.; Felli, F.; Brotzu, A.; Caponero, M.A.; Paolozzi, A. "Improving FBG Sensor Sensitivity at Cryogenic Temperature by Metal Coating". IEEE Sensors Journal, 2008, 8(7), 1299-1304.
20. LakeShore, http://www.lakeshore.com/products/Cryogenic-TemperatureSensors/Pages/ default. aspx. (accessed May 15, 2013).
21. James, S.W.; Tatam, R.P.; Twin, A.; Bateman, R.; Noonan, P. "Cryogenic temperature response of fibre optic long period gratings." Meas. Sci. Technol, 2003, 14(8), 1409-1411.
22. Pinet, E. "Fabry-Pérot Fiber-Optic Sensors for Physical Parameters Measurement in Challenging Conditions." Journal of Sensors, 2009, 2009, 1-9.
23. Bertrand, S.F.; Boulon, G.; Rouhet, J.Y.; Tribillon, G.M. Device for optically measuring a cryogenic temperature. USA Patent US 6086250 A. July 11, 2000.
24. Habisreuther, T.; Hailemichael, E.; Ecke, W.; Latka, I.; Schröder, K. et al. "ORMOCER Coated Fiber-Optic Bragg Grating Sensors at Cryogenic Temperatures." IEEE Sensors Journal, 2012, 12(1), 13-16.
25. Mizunami, T.; Tatehata, H.; Kawashima, H. "High sensitivity cryogenic fibre-Bragg-grating temperature sensors using Teflon substrates." Meas. Sci. Technol., 2001, 12(7), 914–917.
26. Ecke, W.; Latka, I.; Habisreuther, T.; Lingertat, J. "Fiber optic grating sensors for structural health monitoring at cryogenic temperatures." Proc. SPIE, 2007, 6530.
27. Latka, I.; Ecke, W.; Höfer, B.; Habisreuther, T.; Willsch, R. "Fiber optic Bragg gratings as magnetic field-insensitive strain sensors for the surveillance of cryogenic devices." Cryogenics, 2009, 49(9), 490–496.
28. Rajini-Kumar, R.; Suesser, M.; Narayankhedkar, K.G.; Krieg, G. "Fiber Bragg grating sensors for low temperature sensing applications." Proc. 7th Int. Conf. Opt. Technol. (OPTO'06), May 30-Jun. 01 2006, 195-200.

29. Morey, W.W.; Meltz, G.; Glenn, W.H. "Fiber optic Bragg grating sensors." Proc. SPIE, 1989, 1169, 98-107.
30. Rao, Y. "In-fibre Bragg grating sensors." Meas. Sci. Technol., 1997, 8, 355-375.
31. Xue, L.; Liu, J.; Liu, Y.; Jin, L.; Gao, S.; Dong, B.; Zhao, Q.; Dong, X. "Method for enhancing temperature sensitivity of fiber Bragg gratings based on bimetallic sheets." Applied Optics, 2006, 45(31), 8132-8135.
32. Mary, T.A.; Evans, J.S.O.; Vogt, T.; Sleight, A.W. "Negative Thermal Expansion from 0.3 to 1050 Kelvin in ZrW_2O_8." Science, 1996, 272(5258), 90-92.
33. Lightfoot, P.; Woodcock, D.A.; Maple, M.J.; Villaescusa, L.A.; Wright, P.A. "The widespread occurrence of negative thermal expansion in zeolites." Journal of Materials Chemistry, 2001, 11, 212–216.
34. Bullis, W. Murray (1990). "Chapter 6". In O'Mara, W.C.; Herring, R.B.; Hunt, L.P. Handbook of semiconductor silicon technology. Park Ridge, New Jersey: Noyes Publications. p. 431.
35. Chaplot, S. L. "Negative thermal expansion in ZrW_2O_8 – Do we give up the concept of normal mode?" Current Science, 2005, 88(3), 347-349.
36. Szocs, E.; Schwager, F.; Toben, M.; Brese, N. "High-speed Indium Electrodeposition: Efficient, Reliable TIM Technology." 2nd Electronics System-Integration Technology Conference: Greenwich,UK, 1-4 September 2008, 347-350.